Marine Environmental Research 204 (2025) 106919

Contents lists available at ScienceDirect

Marine Environmental Research

journal homepage: www.elsevier.com/locate/marenvrev

"Assessment of potential eutrophication in coastal waters of Gran Canaria: Impact on plankton community under CO_2 depletion"

Jorge J. Santos-Bruña [a,b,*], Nauzet Hernández-Hernández [a], María F. Montero [a], Markel Gómez-Letona [a,c], Moritz Baumann [d], Jan Taucher [d], Carsten Spisla [d], Antonia Thielecke [d,e], Andrea Ludwig [d], Ulf Riebesell [d], Javier Arístegui [a,**]

[a] Instituto de Oceanografía y Cambio Global, IOCAG, Universidad de Las Palmas de Gran Canaria, ULPGC, Spain
[b] Centro Oceanográfico de Málaga, Instituto Español de Oceanografía (IEO-CSIC), Fuengirola, Málaga, Spain
[c] Instituto de Investigacións Mariñas (IIM), CSIC, Vigo, Spain
[d] GEOMAR Helmholtz Centre for Ocean Research, Kiel, Germany
[e] Alfred Wegener Institute for Polar and Marine Research, Bremerhaven, Germany

ARTICLE INFO

Keywords:
Coastal eutrophication
CO2 depletion
Alkalinity enhancement
Ecological impacts
Organic matter dynamics
Mesocosms
Gran Canaria

ABSTRACT

Population growth in coastal tourist areas is leading to enhanced waste production, raising concerns about potential nutrient release increases and the resulting impact on marine ecosystems through eutrophication. Knowledge of the specific impacts of eutrophication on plankton communities in many of these regions is limited, highlighting the need for further research and appropriate environmental management strategies. To help address these gaps, we conducted a 30-day mesocosm study in the coastal waters of Gran Canaria, Canary Islands, a major European tourist destination, and the third most densely populated autonomous community in Spain. With the aim of assessing the effects of nutrient input on biomass, primary production (PP) and recycling processes by phytoplankton, zooplankton, and bacterioplankton, we simulated three nutrient discharge intensities (Low, Medium, and High), with daily additions of 0.1, 1, and 10 μmol L^{-1} of nitrate, respectively, along with phosphate and silicate. We observed that PP, chlorophyll *a* (Chl-a), and biomass increased linearly with nutrient input, except in the High treatment, where CO_2 depletion (<1.0 μmol L^{-1}) and an alkalinity increase (>2500 μmol L^{-1}) resulted in reduced PP. Despite limitations in nitrogen (Control, Low, and Medium) or carbon (High) availability across treatments, which led to stabilized or decreased PP rates and dissolved organic carbon (DOC) concentrations, bacterial degradation remained active in all treatments. This microbial activity resulted in an accumulation of recalcitrant chromophoric dissolved organic matter (CDOM), indicating the resilience of carbon recycling processes under varying nutrient conditions. Furthermore, a clear succession was evident in all enriched treatments, transitioning from an oligotrophic condition dominated by pico- and nanophytoplankton to a eutrophic state primarily composed of diatoms. However, under CO_2 depletion, diatoms experienced a decline in the High treatment, leading to the proliferation of potentially mixotrophic dinoflagellates. Microzooplankton was less sensitive than mesozooplankton to the decrease in prey availability and high pH caused by CO_2 depletion. Interestingly, the Medium treatment showed high efficiency in terms of PP, despite reaching CO_2 levels near of 1.0 μmol L^{-1} by the end of the experiment. PP rates increased from 10 to 100 μg C·L^{-1}·d^{-1} during the first week and remained stable as diatoms predominated throughout the study period. These findings provide valuable insights into the responses of plankton communities to varying nutrient inputs and emphasize the importance of considering the effects of DIC depletion, along with changes in total alkalinity, in eutrophication scenarios as well as in ocean alkalinity enhancement experiments aimed at reducing carbon dioxide emissions.

* Corresponding author. Instituto de Oceanografía y Cambio Global, IOCAG, Universidad de Las Palmas de Gran Canaria, ULPGC, Spain.
** Corresponding author.
E-mail addresses: jorgejuan.santos@ieo.csic.es (J.J. Santos-Bruña), javier.aristegui@ulpgc.es (J. Arístegui).

https://doi.org/10.1016/j.marenvres.2024.106919
Received 27 September 2024; Received in revised form 26 November 2024; Accepted 20 December 2024
Available online 22 December 2024

1. Introduction

One of the significant challenges currently faced by coastal ecosystems due to anthropogenic influence is eutrophication (Howarth, 2008; Howarth and Marino, 2006). The primary cause of this eutrophication is the increase in nitrogen and phosphorus content in water bodies resulting from human-originated discharges (Paerl, 1999; Rabalais et al., 2009). The consequences of these discharges on aquatic ecosystems include high phytoplankton growth rates that disrupt the natural balance of these waters, occasionally affecting their (EU monitor, Directive, 1991/676). Depending on the nutrient loading, negative changes may occur if the nutrient input is excessive (Ferriol et al., 2016), such as harmful micro- and macroalgal blooms (Glibert and Burford, 2017; Feng et al., 2024) or reduced oxygen availability due to increased bacterial respiration rates and decreased light availability for photosynthetic organisms (Correll, 1998). However, under moderate nutrient input, increased algal growth may yield some favourable effects, such as enhanced oxygenation through primary production (Alcántara et al., 2015) or increased biomass transfer in the food web, boosting local fisheries resources and carbon fixation into the ocean (Lin et al., 2014). With the rising human population in tropical and subtropical coastal areas (Benkeblia and Radeva, 2018), archipelagos in these latitudes are at risk of experiencing amplified effects of these disturbances in the coming years. In 2023, the Canary Islands rank as the third most densely populated autonomous community in Spain, following Madrid and the Basque Country, with 293 residents per km^2 and reaching nearly 2.2 million inhabitants with a linear trend for decades (Jerez-Darias and García-Cruz, 2024). Record-breaking numbers of tourists have been registered consistently, exceeding 16 million in 2023 according to data published by the government of Canary Islands (ISTAC, Gobierno de Canarias). This growth both in tourist pressure and the archipelago's population has led to an increase in waste production in recent years. Considering the insularity of the territory and that 27% of this waste is organic (Santamarta et al., 2023), an increase in nutrient content in the archipelago's waters, potentially leading to eutrophication-related effects, can be expected. In addition, the increased exploitation of resources in the archipelago may increase waste products and run-off from agricultural and aquaculture activities (Delgado and Riera, 2020). However, there are still limited studies on the effects of eutrophication in the Canary Islands.

The quantification of the impact of nutrient discharges on the phytoplankton community is essential for managing nutrient releases in coastal areas. One approach to achieve this is with mesocosms that simulate the effects of different nutrient loads (Duarte et al., 2000). Several mesocosm experiments in the waters of the Canary Islands have aimed to simulate upwelling conditions (Baños et al., 2022; Baumann et al., 2021; Gómez-Letona et al., 2022) or ocean acidification (Bach et al., 2019a; Hernández-Hernández et al., 2018) on subtropical planktonic communities. A common outcome in non-limiting mesocosm experiments and natural upwelling conditions is the succession from the subtropical community dominated by pico-nano phytoplankton to micro-nano phytoplankton, with diatoms being the dominant group in terms of primary production (Anabalón et al., 2014; Baños et al., 2022; Hernández-Hernández et al., 2018; Ortiz et al., 2022). However, unlike eutrophication, in natural upwelling or artificial upwelling and acidification in mesocosms, the planktonic community from surface layers experiences an input of dissolved inorganic carbon (DIC). This is due to the upwelling of highly remineralized water or low acid pH values, respectively (Anabalón et al., 2014; Baños et al., 2022; Baumann et al., 2021; Hernández-Hernández et al., 2018). As DIC availability is a crucial factor in altering phytoplankton communities and their primary production rates (Chen and Durbin, 1994; Goldman, 1999), it is imperative to conduct new experiments under conditions like those occurring during eutrophication to accurately assess management methods.

To address this critical knowledge gap, this study focuses on a mesocosm experiment that simulates three different eutrophication conditions, each treatment characterised by a different intensity of nutrient input. By excluding gas injection during the experiment, the research aims to closely replicate the conditions associated with coastal discharges. The main objectives were to analyse the effects of nutrient inputs on the subtropical plankton community, evaluating the impacts on biomass production and recycling processes. This investigation is relevant not only for enhancing our understanding of eutrophication dynamics but also for informing effective and targeted management strategies in coastal areas facing similar challenges. The outcomes of this study provide valuable insights that can guide sustainable practices and policies to safeguard the ecological integrity of coastal ecosystems, particularly in regions like the Canary Islands where the convergence of population growth and tourism intensifies the risk of eutrophication-related disturbances.

2. Material and methods

2.1. Experimental setup

The experiment was conducted from September 1 (T0) to October 1 (T30) of 2017. During this period, eight mesocosms were deployed at the Taliarte pier on the east coast of Gran Canaria. Each cylindrical mesocosm bag had a diameter of 2 m and a length of 2.5 m. They were made of transparent polyurethane foil (PU) to allow solar radiation to penetrate. A conical sediment trap was attached to the bottom of each bag to collect sinking particles, following the design of the larger KOSMOS mesocosm described in Riebesell et al. (2013).

Water used to fill the mesocosms was obtained offshore from the Taliarte pier using a peristaltic pump, at a depth of approximately 3–5 m. To minimize stress on plankton organisms, the pumping speed was maintained at 3.9 L per second. The total isolated volume of each mesocosm was 8 m^3 after filling on day T0 (Fig. 1A). Four different duplicate nutrient treatments (Control, Low, Medium, and High) were implemented to simulate distinct eutrophication intensities during the experiment (Fig. 1B).

Only in the control mesocosms (M1 and M6) no inorganic nutrients were added throughout the experiment. In all other treatments (Low, Medium, and High), inorganic nutrients were added daily from day T4 to T28. The Low treatment mesocosms (M3 and M8) received daily nutrient concentrations of 0.1 μmol L^{-1} of nitrate (N), 0.0063 μmol L^{-1} of phosphate (P), and 0.1 μmol L^{-1} of silicate (Si) from T4 to T6, and 0.05 μmol L^{-1} of Si from T10 to T29. The Medium treatment mesocosms (M4 and M7) received daily nutrient additions of 1 μmol L^{-1} of N, 0.063 μmol L^{-1} of P, and 1 μmol L^{-1} of Si from T4 to T6, and 0.5 μmol L^{-1} of Si from T10 to T29. Finally, the High treatment mesocosms (M2 and M5) received daily nutrient concentrations of 10 μmol L^{-1} of N, 0.63 μmol L^{-1} of P, and 10 μmol L^{-1} of Si from T4 to T6, and 5 μmol L^{-1} of Si from T10 to T29. The nutrient concentrations added to each treatment always followed a Redfield ratio of Si:N:P = 8:16:1 (Fig. 1B). Using this ratio, the levels of N, P and Si are not limiting for phytoplankton uptake and the methodology is comparable, being a standard in nutrient loading studies (Joint et al., 2002; Lagus et al., 2007; Mieczan et al., 2015). The addition of silicate was halted from T7 to T9, and the concentration was adjusted from T10 onwards to maintain the Redfield ratio across all treatments. To prevent the growth of fouling organisms and allow solar radiation to penetrate the mesocosms, the bags were periodically cleaned from the inside on days T4, T8, T16, T20, T24, and T26 using a custom ring with a similar diameter to the bags (Riebesell et al., 2013). Divers also cleaned the outer sides of the mesocosm bags with brushes on days T6, T13, T19, and T25. Water samples were collected daily from all mesocosms for biogeochemical analyses from T1 to T29, while sediment trap and zooplankton samplings were conducted alternating every two days (Fig. 1A).

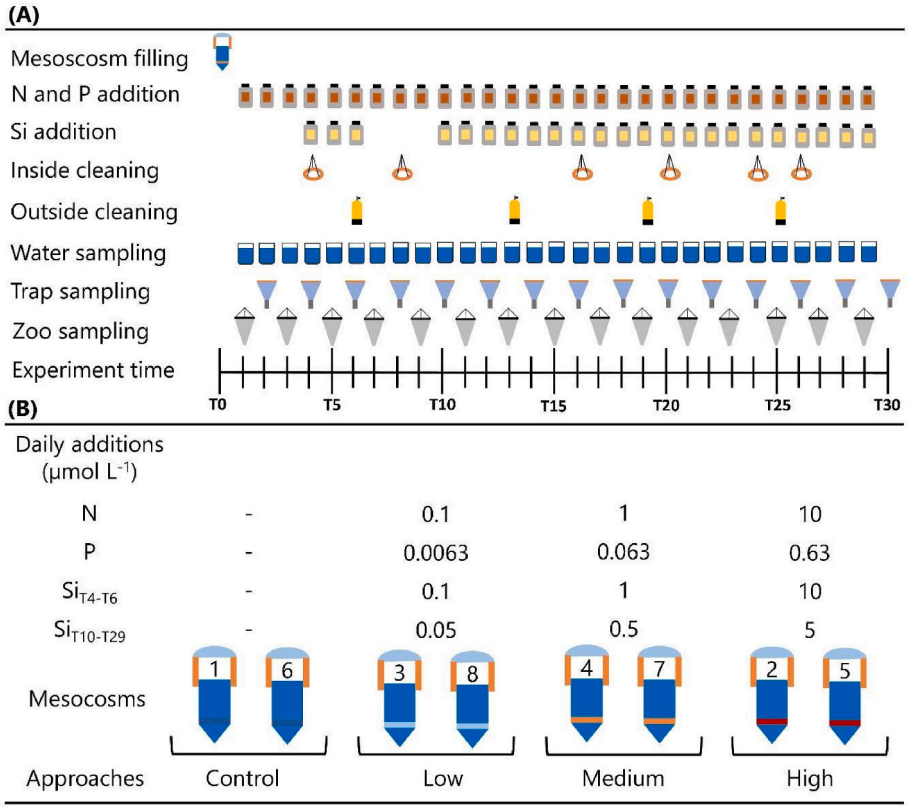

Fig. 1. Experiment chronogram (A), depicting the various tasks performed each day, and the experiment scheme (B), illustrating the nutrient additions carried out in each treatment along with their corresponding mesocosms.

2.2. Nutrients and inorganic carbon

For nutrient analysis triplicate samples of mesocosm water were collected in plastic bottles previously cleaned with 10% HCl. The samples were immediately transported to the laboratory where they were filtered through 0.45 µm cellulose acetate filters (Whatman) before being measured. Concentrations of nitrate, nitrite, phosphate, silicate, and ammonium were measured simultaneously using a SEAL Analytics QuAAtro AutoAnalyzer connected to a JASCO Model FP-2020 Intelligent Fluorescence Detector following Hansen and Grasshoff (1983) and Murphy and Riley (1962). Ammonium concentrations were determined fluorometrically following the method described by Holmes et al. (1999). An autosampler, the SEAL Analytical XY2, was used to inject the water samples into the detection system.

Total alkalinity (TA) was measured in each mesocosm every two days by automated potentiometric titration using an 862 Compact Titrosampler (Metrohm) following Grasshoff et al. (2009). Oxygen, salinity, temperature, and pH were measured using a CTD probe (CTD60M, Sea and Sun Technologies) equipped with the respective sensors, already calibrated, providing daily depth profiles from the surface to close to the bottom of the mesocosms. The values obtained during the CTD profiles were averaged, always achieving a standard deviation below 26% of the mean. From TA and pH, speciation of dissolved inorganic carbon (CO_2, HCO_3^-, and CO_3^{2-}) was calculated using the MS Excel program CO2SYS, Version 01.05, by Pierrot et al. (2006). The carbonate dissociation constants (K1 and K2) from Mehrbach et al. (1973), refit by Dickson and Millero (1987), were used, and input data included temperature and salinity.

2.3. Chlorophyll a and primary production

For each mesocosm, a 500 mL water sample was gently filtered through a polycarbonate filter (Whatman) with a pore size of 0.2 µm, employing low vacuum pressure. The chlorophyll *a* (Chl-a) collected on the filters was extracted by placing them in 10 mL of 90% acetone (volume) at 4 °C for 24 h. Chl-a concentrations were measured fluorometrically using a previously calibrated Turner 10-AU bench fluorometer, following the method described by Holm-Hansen et al. (1965). Primary production (PP) was measured using the ^{14}C method. Four 70 mL water samples, prefiltered with a 200 µm mesh, were collected in Tissue Culture-treated flasks with a growth area of 25 cm^2 (VWR). These samples were transported to the radioactive facilities within 1 h after sampling. Each sample was then supplemented with 15 µCi of ^{14}C-labeled sodium bicarbonate solution ($NaH^{14}CO_3$; PerkinElmer) and incubated *in vitro* for 24 h (with a 12-h day-night cycle) in a light-temperature-controlled chamber. The light intensity and temperature in the chamber were adjusted to replicate the daily average *in situ* conditions.

One out of the four samples was covered with an opaque foil to measure dark carbon uptake. After incubation, a 5 mL aliquot was filtered under low vacuum pressure onto a 0.2 µm pore-size polycarbonate filter using a circular filtration manifold, allowing the filtrate to be collected in a 20 mL scintillation vial. The filters were placed in 10 mL scintillation vials. A second 5 mL aliquot was directly transferred to a new 20 mL scintillation vial. The two liquid samples were acidified with 100 µL of 17.5% HCl and placed in an orbital oscillator for another 24 h, while the filters were exposed to 37% HCl fumes for 24 h. The acidification process aimed to remove the ^{14}C-labeled inorganic carbon from the samples. Finally, 10 mL and 5 mL of Ultima Gold XR scintillation cocktail were added to the 20 mL and 10 mL vials, respectively. The vials were thoroughly mixed and stored in darkness for 24 h. The isotopic disintegrations per minute were measured using a Beckman LS-6500 scintillation counter. PP rates (µg $C{\cdot}L^{-1}$ h^{-1}) were calculated using the following equation.

$$PP = \left[\frac{V_S}{V_f}\right] \cdot \frac{DIC \cdot (DPM_S - DPM_D)}{DPM_A \cdot t_i}$$

where V_s/V_f is the ratio between the sample volume and the filtered volume in L, *DIC* represents the dissolved inorganic carbon concentration in μg C·L^{-1}, DPM_S-DPM_D is the net disintegrations per minute corrected for dark carbon uptake, DPM_A is the initial addition of ^{14}C in disintegrations per minute, and t_i is the incubation time in hours. PP rates obtained from the filters correspond to the particulate PP (PO^{14}C), while the rates obtained from the filtrate and non-filtrate aliquots correspond to the dissolved PP (DO^{14}C) and the total PP (TO^{14}C), respectively.

2.4. Organic matter characterization

At PLOCAN, the sediment trap (ST) material was prepared for elemental analysis of particulate organic carbon (POC) and particulate organic nitrogen (PON) by separating the particles from the seawater. A 3 M solution of ferric chloride ($FeCl_3$) was added to each 5L bottle of sediment material to enhance flocculation and coagulation. This was followed by the addition of a 3 M solution of sodium hydroxide (NaOH) to compensate for the decrease in pH, as described in detail in Boxhammer et al. (2016). After allowing the material to settle for 1 h, the supernatant was gently decanted. The remaining flocculated material was then centrifuged for 10 min at approximately 5200 times gravity (g) using a 6-16 KS centrifuge (Sigma Laborzentrifugen GmbH, Osterode am Harz, Germany). An additional 10-min centrifugation step at approximately 5000 g in a 3K12 centrifuge (Sigma) resulted in compact sediment pellets, which were subsequently frozen at −20 °C and transported to Kiel for further processing. In Kiel, the pellets were freeze-dried to remove any residual moisture and then ground to a fine homogeneous powder suitable for subsampling and elemental analysis using a cell mill (Edmund Bühler GmbH, Bodelshausen, Germany), following the methods described by in Boxhammer et al. (2016). Subsamples for POC/N were weighed into tin capsules, acidified with a 1 M solution of HCl, dried overnight at 50 °C, and then measured in duplicate using a CN analyzer (Euro EA-CN, HEKAtech GmbH, Wegberg, Germany) according to Sharp (1974).

Water column samples were collected in our onshore laboratories and subsampled for POC and PON by filtering them onto pre-combusted glass fibre filters (0.7 μm of nominal pore, Whatman). The POC and PON filters underwent acidification for approximately 2 h using a 1 M solution of HCl to eliminate any inorganic carbon. After acidification, the filters were dried overnight at 60 °C in pre-combusted glass Petri dishes. Filters intended for total particulate carbon (TPC) were dried without prior acidification. All filters were then packed into tin cups (8 × 8 × 15 mm, LabNeed GmbH, Nidderau, Germany) and brought to Kiel for analysis. In Kiel, the filters were analyzed for carbon and nitrogen content using a CN analyser (Euro EA-CN, HEKAtech), following the same procedure as described above for the sediment samples. In some cases, due to errors in sample handling or measurements, the measured POC concentrations were higher than those of TPC. Whenever the difference exceeded 10%, we reported the TPC concentration instead of the POC concentration, assuming the absence of particulate inorganic carbon.

For the measurement of DOC, 10 mL of filtered samples were stored in high-density polyethylene bottles and frozen at −20 °C until analysis. The samples were then analyzed using a Shimadzu TOC-5000 analyser (Sharp et al., 1993). Prior to analysis, the samples were thawed and acidified with 50 mL of 50% H_3PO_4. They were then purged with CO_2-free air for several minutes to remove any inorganic carbon. The concentration of DOC was determined by referencing standard curves of potassium hydrogen phthalate, ranging from 30 to 200 μM, which were prepared daily (Thomas et al., 1995).

Absorbance spectra of the dissolved organic matter (DOM) were measured using a JASCO V-750 spectrophotometer with 10 cm path length quartz cells. Each sample was subjected to absorbance measurements across a wavelength spectrum ranging from 250 nm to 750 nm (at increments of 0.5 nm). Before and after sample measurements, a blank measurement was conducted using ultrapure Milli-Q water. The mean of blank spectra from each day were then subtracted from the sample spectra, and a baseline correction was applied by subtracting the average absorbance of each sample between 600 nm and 700 nm from the entire spectrum. After these processing steps, the absorbance values were converted to Napierian absorption units as defined by the equation:

$$a_\lambda = 2.303 \cdot \frac{Abs_\lambda}{L}$$

where, for each wavelength λ, the absorption coefficient a_λ is given by the absorbance at wavelength λ (Abs_λ), the path length (*L*, in meters; here 0.1) and 2.303 (the constant that converts from decadic to natural logarithms). The spectral value at 325 nm was considered as a proxy for the concentration of chromophoric dissolved organic matter (CDOM), while the slope of the natural-log-transformed spectra between 275 nm and 295 nm has been shown to be highly sensitive to changes in the molecular weight of CDOM and transformation of organic matter by microbes (Catalá et al., 2018; Helms et al., 2008).

2.5. Plankton community structure and biomass estimates

Pigmented picoplankton and nanoplankton cells were counted *in vivo* using a FACScalibur (Becton and Dickinson) flow cytometer within 3 h after subsampling from the water samples. Due to the large size differences between the groups, flow cytometer settings were adjusted for each size group. Picoplankton samples (1.8 mL) and nanoplankton samples (3.6 mL) were collected in cryovials (2 mL and 4 mL, respectively) and stored in darkness at 4 °C until analysis. For picoplankton samples, a suspension of yellow-green 1 μm latex beads (Polyscience, Inc.) at a concentration of approximately 10^5 beads/mL was added as an internal standard. The samples were then run at a flow rate of 75 μL min^{-1} for 150 s. In the case of nanoplankton samples, red latex beads with a diameter of 2 μm (~105 beads mL^{-1}) (Polyscience, Inc.) were used as the internal standard, and the samples were run at a flow rate of 335 μL min^{-1} for 300 s. Two picoplankton groups, *Synechococcus* (Syn [~1 μm]) and picoeukaryotes (PEuk [~2 μm]), as well as two nanoeukaryote groups (NEuk1 [2–10 μm] and NEuk2 [10–20 μm]), were identified based on their signatures in side scatter (SSC) vs red (FL3) and orange (FL2) fluorescence bivariate plots.

Microplankton (diatoms, dinoflagellates, and microzooplankton) were sampled using brown glass bottles and immediately fixed with alkaline lugol iodine (1% final concentration). Subsamples were allowed to sediment for at least 24 h in 100 mL Utermöhl chambers before being counted using an inverted microscope (Utermöhl, 1931). Heterotrophic bacteria (HB) were fixed with a final concentration of 2% formaldehyde after being kept at 4 °C for 30 min and then stored frozen in liquid nitrogen until flow cytometer analysis. Subsamples (400 μL) were stained with the fluorochrome SYBR Green I, Molecular Probes (final concentration 1000 × dilution of the commercial product), at room temperature before analysis. HB were identified based on their signatures in a plot of SSC versus green fluorescence (FL1).

Samples were run at a low speed for HB (16 μL min^{-1}). To estimate the sizes of pico and nanoplankton cells, the flow cytometer was calibrated using nonfluorescent latex beads of various sizes (1, 2, 4, 6, 10, and 15 μm in diameter) from Molecular Probes. The side scatter (SSC) values obtained from the calibration beads were normalized to the SSC measured for fluorescence standard beads added to every sample (1 μm for picoplankton settings and 2 μm for nanoplankton settings). Linear regression analyses were performed between the bead diameters and normalized SSC values for picoplankton (ø = 9.914 · log (SSC) - 0.219; $R^2 = 0.92$) and nanoplankton settings (ø = 4.753 · log (SSC) + 0.008; R^2

= 0.93). Cell diameters (μm) were inferred from the normalized SSC values for each group and then used to calculate cell biovolume (μm^3) assuming a spherical shape. The carbon content (biomass) of the cells was estimated using the following conversion factors: 230 fg C·μm^{-3} for Synechococcus (Bjørnsen, 1986), 237 fg C·μm^{-3} for picoeukaryotes (Bjørnsen, 1986), and 220 fg C·μm^{-3} for nanoeukaryotes (Børsheim and Bratbak, 1987). For microplankton cell volumes, calculations were performed following the methodology described by Olenina et al. (2006) whenever possible. The conversion from volume to biomass was done using the equations provided by Menden-Deuer and Lessard (2000).

For mesozooplankton biomass, organisms were meticulously hand-picked from samples collected using vertical net hauls with an Apstein net (55 μm mesh size, ø 17 cm, HYDRO-BIOS Kiel) every two days (from T1 to T29). The organisms were dried at approximately 60 °C for at least 24 h, placed into tin capsules, and stored in a desiccator until analysis on a carbon/nitrogen analyser (GEOMAR Kiel, Thermo Scientific IRMS).

2.6. Statistics

Non-parametric Friedman tests were conducted to determine statistical differences in PP, biomass, and nutrient consumption values among the different treatments in the experiment. The choice of a non-parametric analysis was made because the data violated the assumptions of normality and homoscedasticity, making repeated measures ANOVA inappropriate (Zimmerman and Zumbo, 1993). Additionally, linear regressions were performed to examine the relationships between CO_2 values and PP for the different treatments. The assumptions of normality and homoscedasticity for the regressions were assessed using Q-Q plots and residual vs fitted variable plots respectively (Schützenmeister et al., 2012). All graphical and statistical analyses were carried out using the R statistical software (Version 4.3.0).

3. Results

3.1. Inorganic nutrients and CO_2 evolution

An increase in the concentration of the added nutrients (N, P, and Si) was observed in the mesocosms during the first days, which peaked and then decreased due to rapid consumption in the Medium and High intensity treatments. However, the concentration peaks were 2–3 times higher in the Medium treatment compared to the High treatment. Additionally, the consumption of nutrients began 5 days earlier in the Medium treatment compared to the High treatment (Fig. 2A–D, E). In the Medium treatment, the nutrients started to be depleted at T6 and continued to decrease until the end of the experiment. However, in the High treatment, the nutrients began to accumulate after day 11 and continued to increase until the end of the experiment. (Fig. 2A–D, E). No nutrient accumulation was observed in the Control and Low treatments at any stage of the experiment. However, differences were observed between the concentrations of nitrate or nitrite (Fig. 2A and B) compared to phosphate or silicic acid (Fig. 2E–D). Nitrate and nitrite showed a constant consumption, characterised by concentration values around 0 in most treatments throughout the experiment, while phosphate and silicic acid showed a linear decrease in the Control and Low treatments until the end. Dissolved oxygen (Fig. 2F) showed a stable trend in the Control and Low treatments throughout the experiment, while the trend was increasing in the High and Medium treatments. Although the rate of oxygen increase was more gradual in the Medium treatment than in the High treatment at the start, oxygen levels in the Medium treatment remained high until the end of the experiment. In contrast, from day 10 onwards in the High treatment, oxygen concentration dropped, reaching values similar to those at the beginning.

A linear increase in TA is observed in all treatments from the

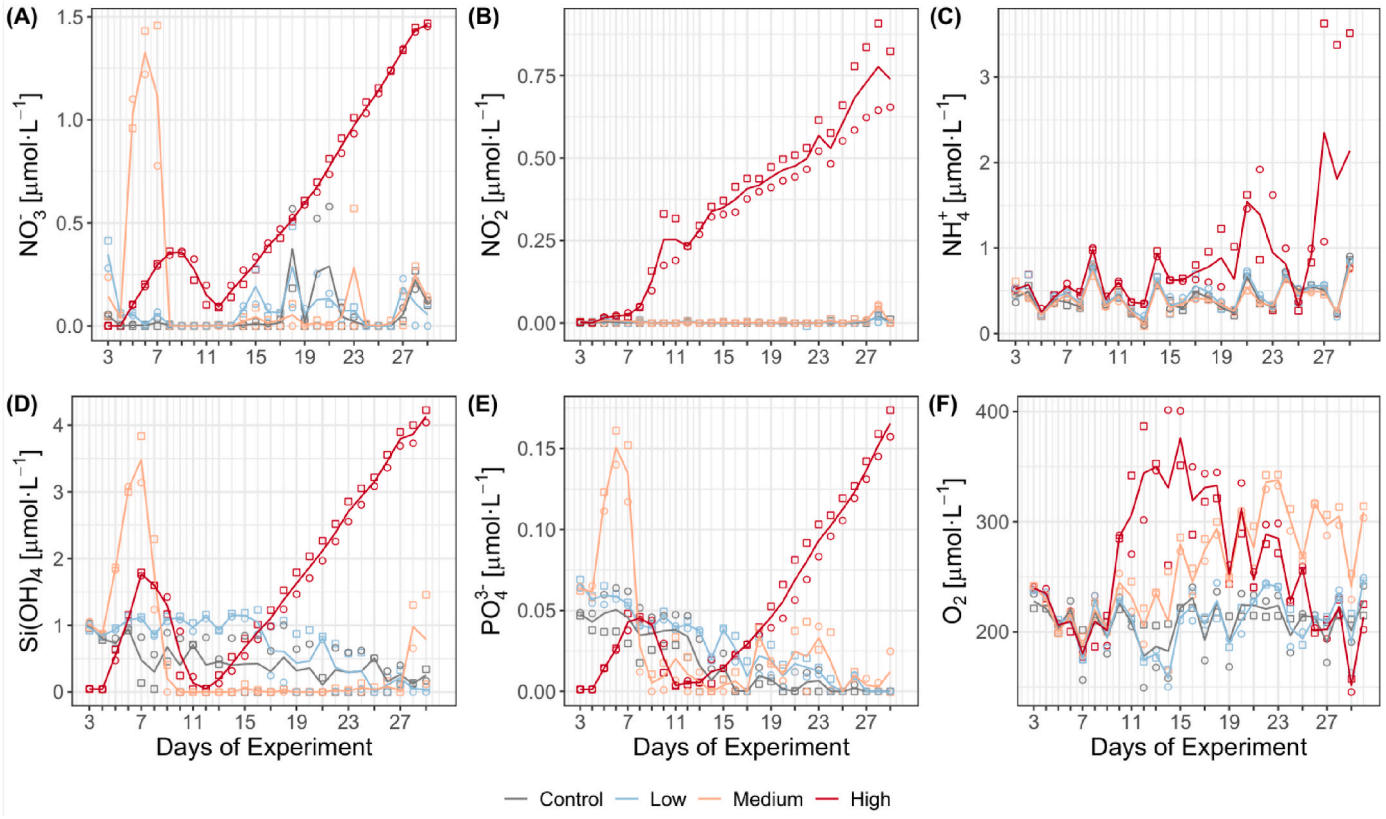

Fig. 2. Dissolved inorganic nutrient concentration during the experiment, with treatments distinguished by colour and mesocosms by shape. The line represents the mean value between both mesocosms. The panels are labeled as follows: (A) Nitrate, (B) Nitrite, (C) Ammonium, (D) Silicic acid, (E) Phosphate, and (F) Oxygen. (For interpretation of the references to colour in this figure legend, the reader is referred to the Web version of this article.)

beginning to the end of the experiment (Fig. 3A). However, the slope of this regression seems to be proportional to the nutrient input. The maximum TA values at the end of the experiment in the different treatments were approximately 2580 µmol·L-1 in the High, 2515 µmol·L-1 in the Medium, 2475 µmol·L-1 in the Low, and 2465 µmol·L-1 in the Control. Values from pH underwent significant changes in the Medium and High treatments from the first third of the experiment onwards (Fig. 3B). In the Medium treatment, the pH progressively increased from a value of 8.3 on day 10, reaching approximately 8.8 at the end of the experiment. The values in the second half of the experiment in this treatment remained above 8.5. In contrast, in the High treatment, the pH increased abruptly a few days before the Medium treatment, ranging from 8.2 to 9 in the second half of the experiment. The remaining treatments maintained constant values around 8.2.

The data for CO_2 and HCO_3^- revealed a logistic depletion pattern in the Medium and High treatments, with a more pronounced decrease for CO_2 (Fig. 3C–E). In the High treatment, the depletion rate of CO_2 was steeper, stabilising around 0.5 µmol L^{-1} by day 13, while HCO_3^- showed a slight increase towards the end, reaching approximately 750 µmol L^{-1}. In contrast, the Medium treatment exhibited a gentler decline, with CO_2 and HCO_3^- concentrations reaching values above 1.0 µmol L^{-1} and 900 µmol L^{-1}, respectively, by the end of the experiment. The Control treatment showed minimal variation in CO_2 and HCO_3^- levels, while the Low treatment displayed a slight linear decrease in CO_2 only, ending with values above 7.5 µmol L^{-1}. The CO_3^{2-} data followed a similar pattern to HCO_3^- but in an inverse manner (Fig. 3E). In the High treatment, CO_3^{2-} concentrations increased until day 15, where they stabilized and eventually reached approximately 700 µmol L^{-1} by the experiment's end. The Medium treatment showed a linear increase in CO_3^{2-}, reaching around 600 µmol L^{-1} at the conclusion. In the Control and Low treatments, CO_3^{2-} concentrations remained relatively unchanged throughout the experiment.

3.2. Chlorophyll a and primary production evolution

The PP rates and Chl-a concentration exhibited rapid increases during the initial 10 days of the experiment in nearly all treatments, with minimal or no increase observed in the Control treatment (Fig. 4). Following this phase, which coincided with the accumulation of nutrients in the High treatment, Chl-a values and PP rates in Control and Low reached a stable state with slight fluctuations, ultimately concluding with further growth in most treatments. The magnitude of the values at which PP rates and Chl-a stabilized followed the intensities of nutrient additions. Notably, the High treatment failed to achieve stability and instead experienced a sharp decline in PP rates and Chl-a from day 11 until the conclusion of the experiment. Consequently, the High treatment yielded lower final Chl-a values relative to the Medium treatment and displayed PP rates that were comparable or even lower than those of the Control and Low treatments (Fig. 4).

The Friedman test showed that there were no significant differences ($p > 0.05$) between the Control-Low and Medium-High treatment pairs in terms of total PP (Fig. 5A). However, in the High treatment, linear correlations were observed between the rates of total PP and CO_2 after day 10 of the experiment (Fig. 5B).

In the enriched systems (Low, Medium, High), there was an exponential increase of particulate organic matter concentrations (POC and PON) in both the sediment trap and water column data during the initial 10 days of the experiment (Fig. 6A, B, C and D). After this initial phase,

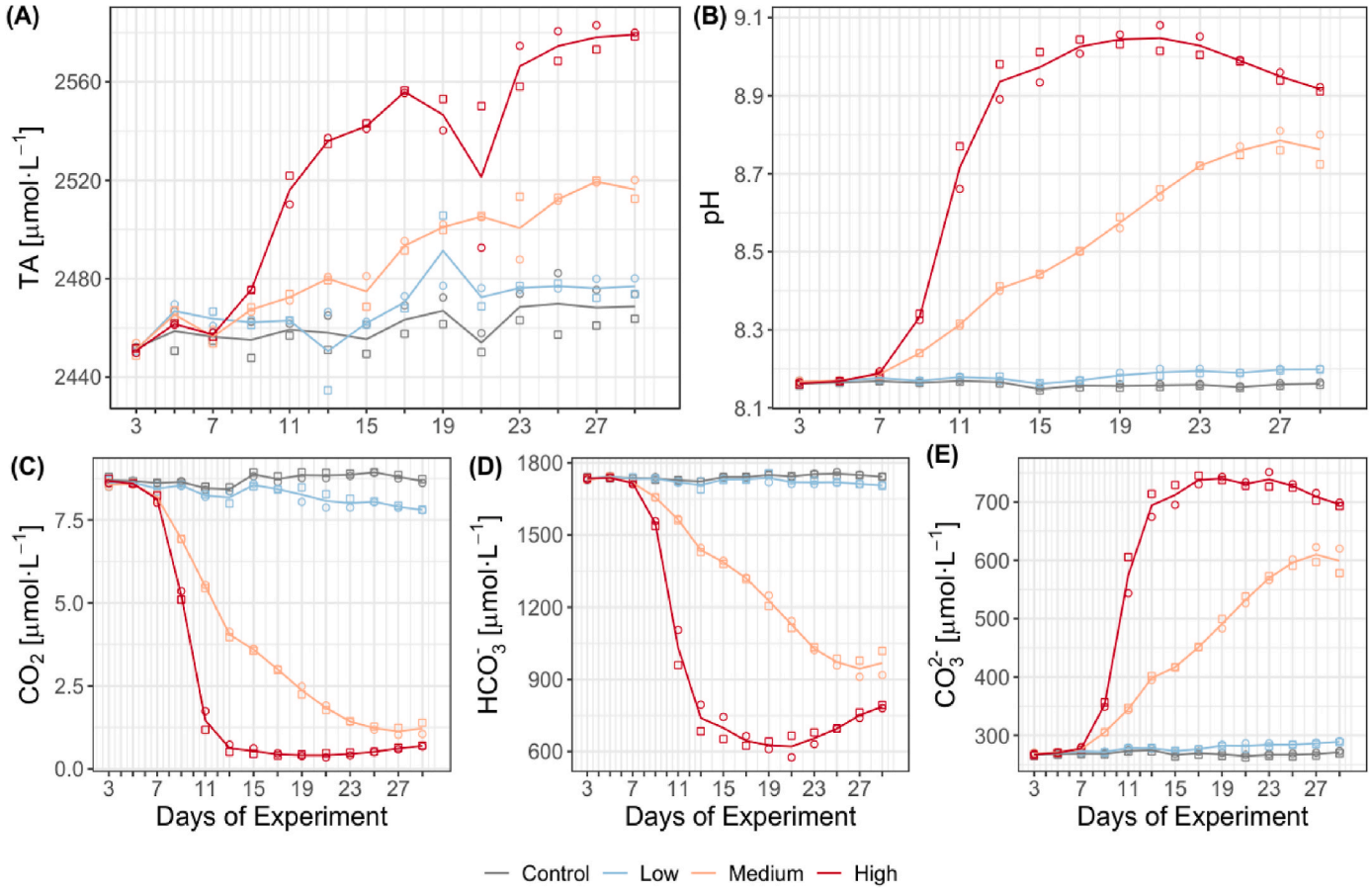

Fig. 3. Time series of total alkalinity (A), pH (B), carbon dioxide (C), bicarbonate (D), and carbonate (E) with treatments distinguished by color and mesocosms by shape. The line shows the mean between the two mesocosms. (For interpretation of the references to colour in this figure legend, the reader is referred to the Web version of this article.)

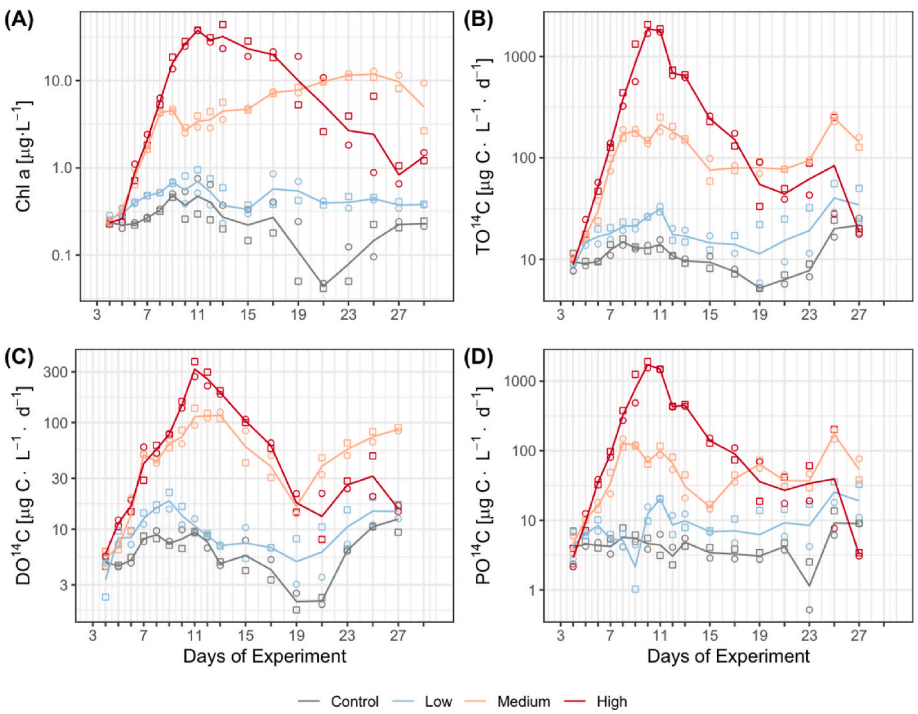

Fig. 4. Evolution of chlorophyll *a* (Chl-a) concentration and primary production (PP) rates throughout the experiment, with treatments differentiated by colour and mesocosms represented by shape. The solid line represents the mean value between both mesocosms. (A) Chl-a concentration. (B) Total PP ($TO^{14}C$). (C) Dissolved PP ($DO^{14}C$). (D) Particulate PP ($PO^{14}C$). Note that the y-axes are in logarithmic scale. (For interpretation of the references to colour in this figure legend, the reader is referred to the Web version of this article.)

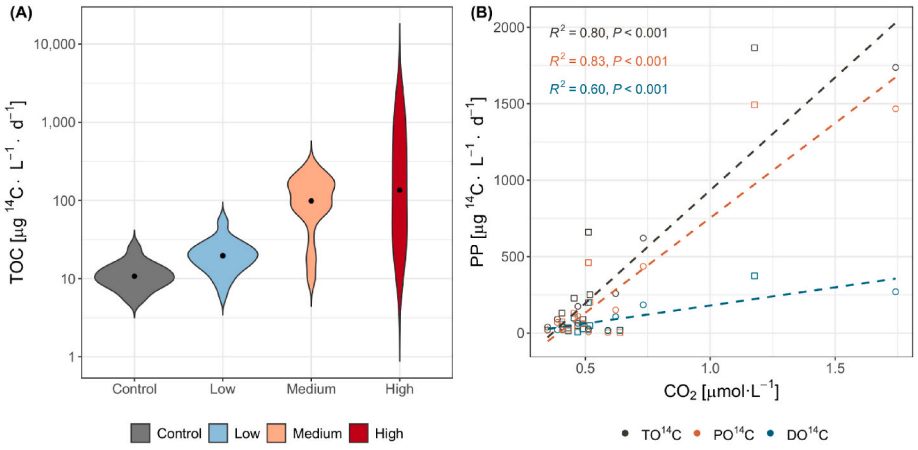

Fig. 5. (A) Violin plot showcasing the PP rates of $TO^{14}C$ for each treatment throughout the entire experiment. Means of each treatment are denoted by black dots. Note that y-axis is in logarithmic scale. (B) Linear regressions between $TO^{14}C$, $PO^{14}C$, $DO^{14}C$ rates and CO_2 concentration in the High treatment. The regressions were conducted with the data obtained from day 10 until the end of the experiment. The data points are distinguished by the colour representing the fraction of organic carbon, and the shape represents the mesocosm of the treatment. (For interpretation of the references to colour in this figure legend, the reader is referred to the Web version of this article.)

POC and PON concentrations appeared to stabilize in almost all treatments, with the trends of Low and Medium treatments in trap values showing a slightly more exponential pattern (Fig. 6A and C). However, in the Medium treatment, the POC and PON values measured in the water column exhibited a constant growth throughout most of the experiment (Fig. 6A–C, and E).

In the High treatment, there was a tendency for both the POC and PON concentrations to decrease after day 10, both in the water column and sediment traps. These final concentrations were lower than those observed in the Medium treatment. In terms of the POC/PON ratios (Fig. 6E and F), most treatments exhibited a relatively stable pattern. However, in the High treatment, after the first week of the experiment, the ratios reached the lowest values and stabilized between 4 and 8 until the end. On the other hand, the other treatments showed significant fluctuations without a clear discernible trend, except for the Medium treatment, which exhibited a logarithmic growth in the water column ratio from day 10 onwards. This growth led to final values of 12 for the water column ratio in the Medium treatment (Fig. 6F).

3.3. Bacterial evolution and their relationship with organic carbon

In contrast to the dissolved PP shown in Fig. 4C, the concentration of

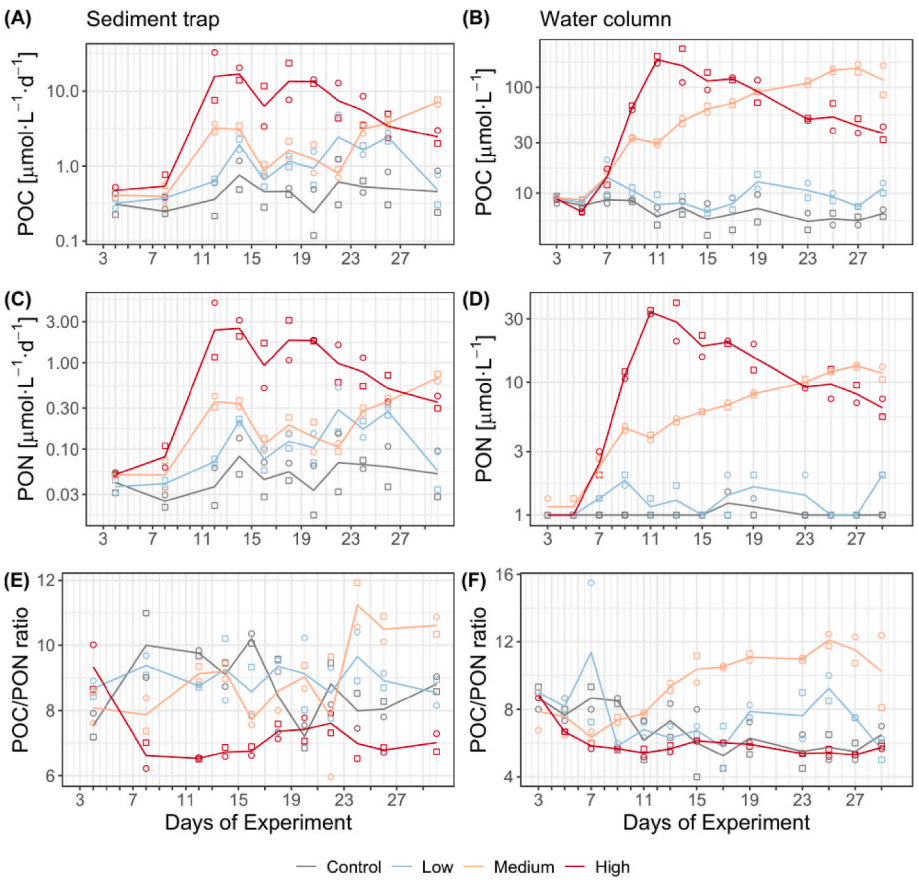

Fig. 6. Time series of particulate organic carbon (POC) and nitrogen (PON), and their ratios (POC/PON) in sediment traps (A, C, and E) and the water column (B, D, and F), with treatments distinguished by colour and mesocosms by shape. The line shows the mean between the two mesocosms. Note that y-axes from A, B, C, and D are in logarithmic scale. (For interpretation of the references to colour in this figure legend, the reader is referred to the Web version of this article.)

DOC displayed a linear trend from day 8 onwards, which was proportional to the treatment intensity (Fig. 7A). However, similar to the PP rates, the High treatment experienced a decline in DOC concentration from day 10 onwards, resulting in lower values compared to the Medium treatment by the end of the 30-day period.

Despite this decline in DOC concentration, heterotrophic bacterial abundance (HB) did not follow the same pattern (Fig. 7B). The trend remained linear for the Medium and High treatments until the end, with no apparent difference in abundance between the two. In the Control and Low treatments, HB abundance reached 10^6 cells·mL^{-1} at the end of the first week but subsequently dropped below 10^3 cells·mL^{-1} and stabilized until the end of the experiment.

Regarding the CDOM, the a_{325} consistently increased over time, with a magnitude proportional to the intensity of the nutrient additions (Fig. 7C). In this case, unlike HB abundance, there was a clear distinction between the values of the Medium and High treatments. The spectral slope between 275 and 295 nm showed an opposite relationship with time (Fig. 7D), with a decreasing trend over the experiment. Similarly to DOC and a_{325}, $S_{275\text{-}295}$ values were related to treatment intensity, High mesocosms displaying the lowest values. Control and Low treatments overall present low variability for these parameters (Fig. 7).

3.4. Trends in phytoplankton community structure

The total biomass throughout the experiment followed a similar trend to the one previously observed for Chl-a or water column POM. Apart from the Control treatment, all other treatments showed an initial increase in total biomass concentration. However, the Low treatment was the first to stabilize (Fig. 8A). The Control treatment exhibited a negative trend in total biomass concentration until the end of the experiment. The total biomass concentration data for the Low and Medium treatments experienced a decrease between days 10 and 20. Subsequently, the Low treatment stabilized at approximately 100 µg C·L^{-1} until the end of the experiment, while the Medium treatment maintained a positive trend with the highest final values. The High treatment initially reached the highest concentration values and showed the most marked increase during the first few days. However, the trend reversed after day 15, and the average final values dropped below 1000 µg C·L^{-1}. The Friedman test used to compare total biomass concentration between treatments did not reveal any significant differences between the pairs Control-Low and Medium-High ($p > 0.05$). The mean values of different approaches with respect to concentration were displayed according to the treatment intensity (Fig. 8B).

The peak in picophytoplankton biomass, represented by *Synechococcus* and picoeukaryotes, occurred between days 7 and 9 (Fig. 9A and B). This peak contributed to over 30% of the total biomass (Fig. 10A). While the Medium and High treatments exhibited the highest biomass values for this phytoplankton fraction during the peak, the percentage of total biomass in these treatments did not exceed 25% (Fig. 10C and D).

From day 11 onwards, the Control and Low treatments showed the highest values for *Synechococcus* biomass, with the Control treatment reaching values above 30 µg C L^{-1} between days 15 and 19 (Fig. 10A). These values represented over 50% of the total biomass in the second half of the experiment (Fig. 10A). Regarding picoeukaryotes, the Medium and Low treatments respectively reached higher biomass concentration values after the peak for this group. However, even in these treatments, picoeukaryotes never represented more than a quarter of the total biomass at any point in the experiment. After the peak on day 9, the High treatment experienced a negative trend, reaching the lowest values by the end of the experiment (Fig. 9B).

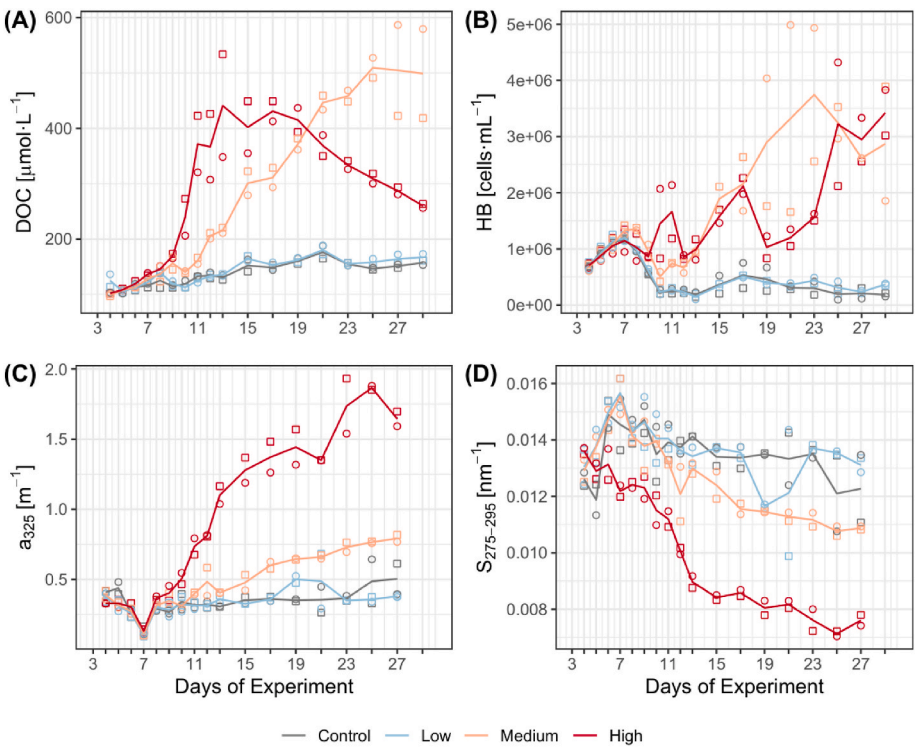

Fig. 7. Time series data with treatments differentiated by colour and mesocosms represented by shape. The lines in the plots indicate the mean values between the two mesocosms. (A) Total dissolved organic carbon (DOC), (B) Heterotrophic bacteria (HB). (C) Absorption coefficient at a wavelength of 325 nm (a_{325}), and (D) Spectral slope for the wavelength band between 275 nm and 295 nm ($S_{275\text{-}295}$). (For interpretation of the references to colour in this figure legend, the reader is referred to the Web version of this article.)

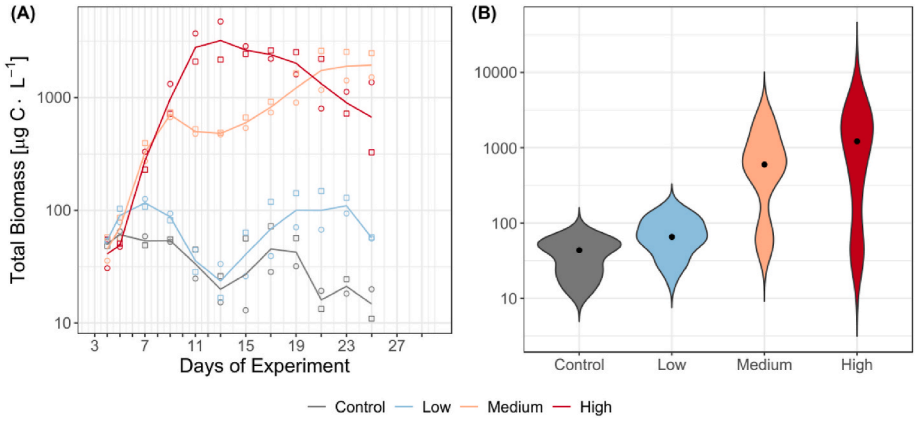

Fig. 8. (A) Time series of total phytoplankton biomass concentration in µg C·L^{-1}, with treatments distinguished by color and mesocosms by shape. The line represents the mean value between both mesocosms. (B) Violin plot of the total biomass concentration for each treatment throughout the entire experiment, with black dots indicating the mean values. Note that the y-axes are in logarithmic scale. (For interpretation of the references to colour in this figure legend, the reader is referred to the Web version of this article.)

The smaller fraction of nanoeukaryotes displayed a biomass concentration peak at T11 (1000 µg C·L^{-1}) that decreased during the rest of the experiment until reach similar values to the Low treatment at T27. Still, in the High treatment the nanophytoplankton represented over 50% of the total biomass for most of the experiment (Fig. 10D). In the Medium treatment, the trend was positive throughout the experiment with final values above 1000 µg C·L^{-1}. Both fractions of nanoeukaryotes in the Low and Control treatments followed a relatively constant trend during the experiment, with values around 10 µg C·L^{-1} (Fig. 9C and D). However, in both treatments, the highest percentages of biomass represented by the nano fraction occurred during the first half of the experiment, due to the growth of *Synechococcus* in the second half of the Control treatment (Fig. 10A) and the increase in diatom biomass in the Low treatment (Fig. 10B). In the larger nanoeukaryote fraction (Fig. 9D), the High treatment did not show a negative trend until after day 20 of the experiment, with stable values above 1000 µg C·L^{-1} from day 10. In the case of the Medium treatment, the growth of the larger nanoeukaryote biomass throughout the experiment was not as pronounced as with the smaller fraction, yet this was the treatment with the highest concentration values for both size fractions at the end of the experiment (Fig. 9C and D).

Lastly, diatoms and dinoflagellates (Fig. 9E and F) remained overall constant in the Control treatment with low biomass concentration throughout the experiment (~1 µg C·L^{-1}). In the first half of the

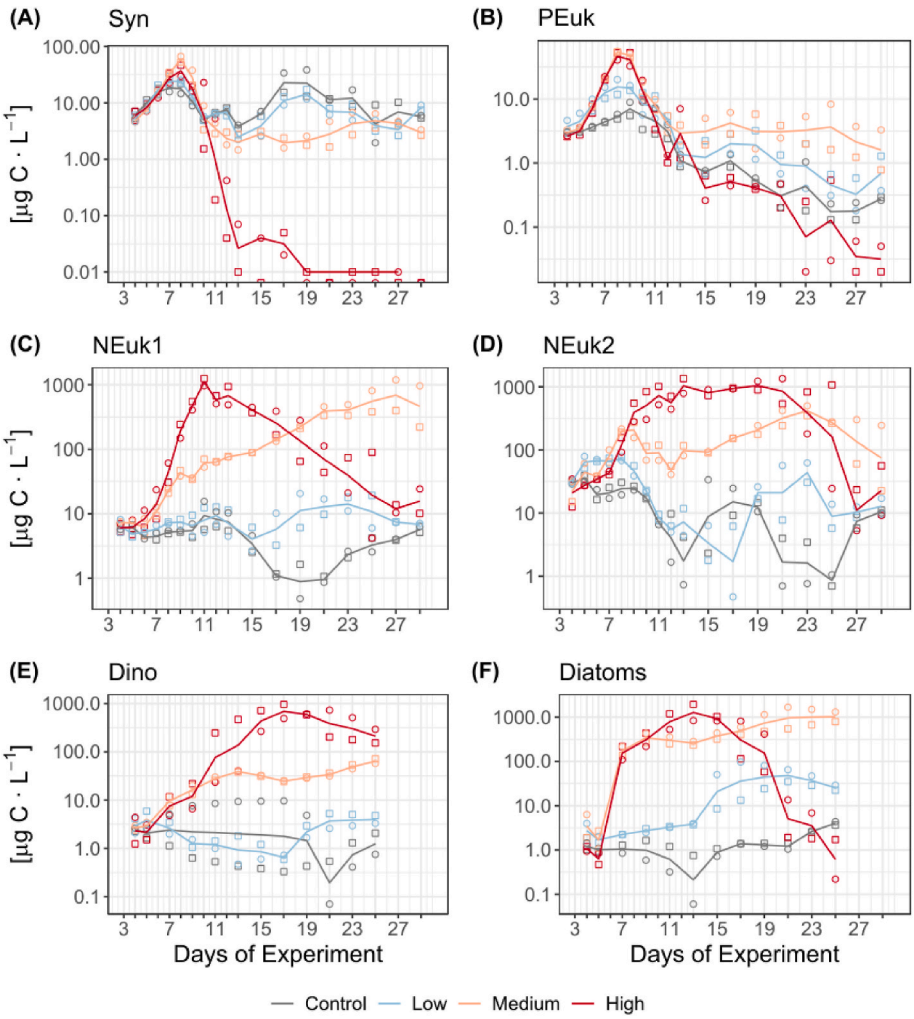

Fig. 9. Time series of phytoplankton biomasses, with treatments and mesocosms distinguished by color and shape. The lines represent the mean values between the two mesocosms. The specific phytoplankton groups shown are as follows: (A) *Synechococcus* (Syn), (B) Picoeukaryotes (PEuk), (C) Nanoeukaryotes (Neuk1; 2–10 µm), (D) Nanoeukaryotes (Neuk2; 10–20 µm), (E) Dinoflagellates (Dino), and (F) Diatoms. Note that the y-axes are in logarithmic scale. (For interpretation of the references to colour in this figure legend, the reader is referred to the Web version of this article.)

experiment, the Low treatment did not show significantly different values from the Control; however, after day 17 in the case of dinoflagellates (Fig. 9E) and day 13 in the case of diatoms (Fig. 9F), the biomass concentrations appeared to increase for both groups, slightly differentiating from the Control treatment, and ended up representing 50% of the total biomass for most of the second half of the experiment (Fig. 10C).

In the case of the Medium and High treatments, the positive trend was evident for dinoflagellates. This increase extended throughout the experiment for the Medium treatment but only until day 17 for the High one, which displayed decreases towards the end. Still, it managed to be the treatment with the highest final biomass concentration for this group, being the only one in which dinoflagellates represented over 25% of the total biomass (Fig. 10D). Diatoms showed a markedly different trend. Between days 5 and 7, in the Medium and High treatments diatom biomass sharply increased to values above 100 µg C·L^{-1}. Subsequently, the trend continued to be positive, albeit with lower increases that were maintained until the end of the experiment for the Medium intensity and ended on day 13 for the High intensity. In the latter, the diatom biomass declined rapidly during the second half of the experiment, ending with values below the Control treatment. In contrast, in the Medium treatment diatom biomass remained above 50% from the first week until the end of the experiment, with concentration values above 100 µg C·L^{-1}, reaching 1000 µg C·L^{-1} by the end of the experiment (Fig. 9F).

3.5. Transfer to zooplankton community

The evolution of zooplankton biomass shows a different behaviour between the microplankton and mesoplankton communities (Fig. 11). While in the microzooplankton community the biomass of the Control and Low treatments does not seem to grow throughout the experiment (Fig. 11A), in the mesoplankton community a linear growth is observed until about day 13, where it seems a decline until the end of the experiment reaching at the values below the Low treatment. The Low treatment ends the experiment with the highest mean biomass among treatments above 10000 µg C· L^{-1} for mesozooplankton (Fig. 11B). Although the High treatment shows positive trends in both fractions at the beginning of the experiment, its evolution ends in a decline from day 17 for microplankton and from day 11 for mesoplankton fractions, becoming the treatment with the lowest mean biomass in the last one (Fig. 11B).

4. Discussion

4.1. Extreme fertilization leads to inorganic carbon depletion

Other mesocosm experiments in which nutrient additions were carried out in a similar manner (Duarte et al., 2000; Ortiz et al., 2022) demonstrate how, at the beginning of the treatments, the added

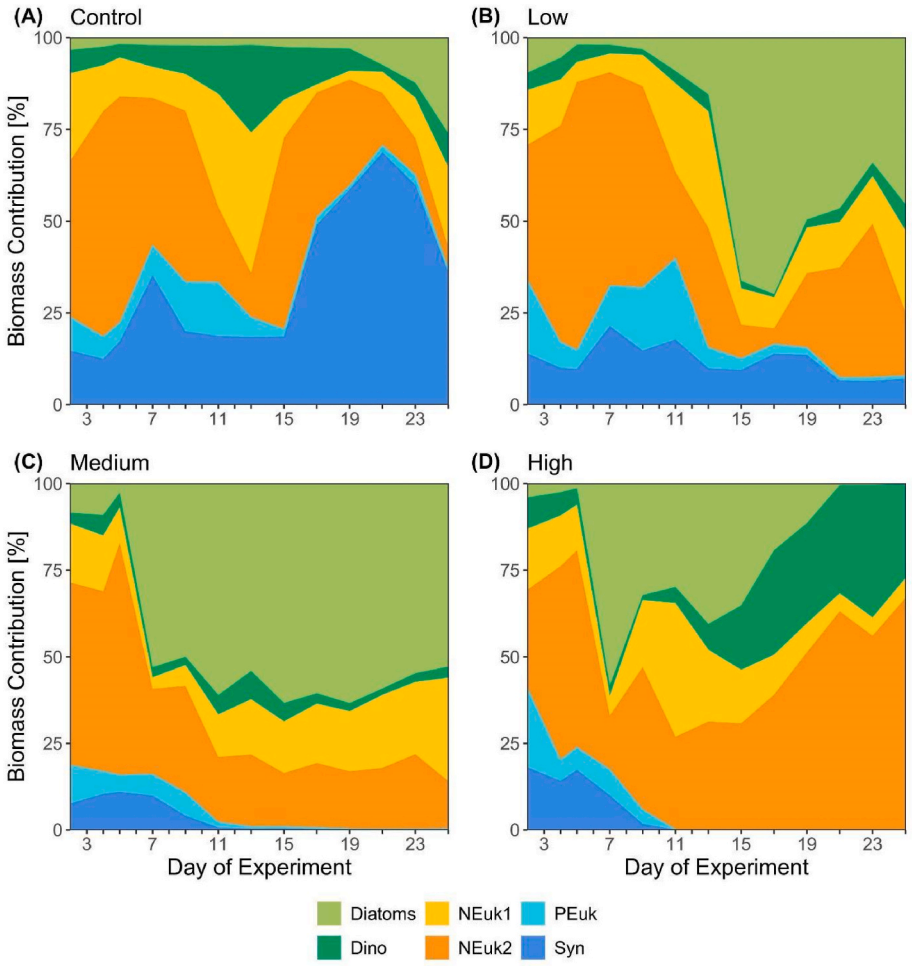

Fig. 10. Stacked area plots showing the percentage contribution of each phytoplankton group in each treatment, distinguished by color (Diatoms, Dino = Dinoflagellates, NEuk1 = Nanoeukaryotes 2–10 μm, NEuk2 = Nanoeukaryotes 10–20 μm, PEuk = Picoeukaryotes, Syn = *Synechococcus*). (A) Control treatment. (B) Low treatment. (C) Medium treatment. (D) High treatment. (For interpretation of the references to colour in this figure legend, the reader is referred to the Web version of this article.)

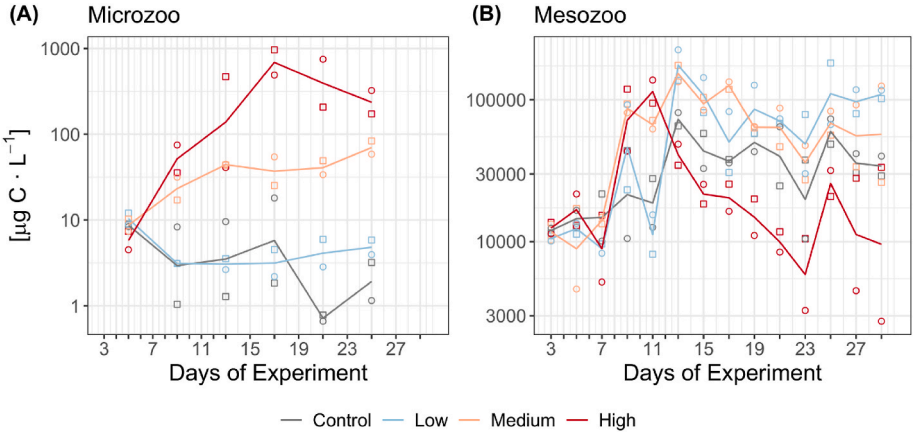

Fig. 11. Time series of zooplankton biomasses, with treatments and mesocosms distinguished by color and shape. The lines represent the mean values between the two mesocosms. The specific zooplankton sizes shown are as follows: (A) Microzooplankton (Microzoo), (B) Mesozooplankton (Mesozoo). Note that the y-axes are in logarithmic scale. (For interpretation of the references to colour in this figure legend, the reader is referred to the Web version of this article.)

nutrients accumulate during the initial days. This first phase serves as acclimation for the planktonic community to the new nutrient availability before their consumption in the following days (Fig. 2A–D and E). However, an imbalance between the availability and replenishment of several essential elements can lead to the depletion of the most limiting one. This is what occurred in the High treatment after the consumption of the added nutrients between days 7 and 11, where CO_2 dropped abruptly to concentrations below 1.25 μmol L^{-1} in just 5 days (Fig. 3C).

The substantial daily nutrient input, combined with a limited gas exchange between the surface and the mesocosms, generated this imbalance that triggered the rapid depletion of available inorganic carbon. In aquatic systems, the high uptake of CO_2 and HCO_3^- by the photosynthetic activity shifts the carbonate system towards the formation of CO_3^{2-}, thereby increasing TA in the system (Shiraiwa et al., 1993), as seen in Fig. 3. Furthermore, proton consumption during photosynthesis (Zerveas et al., 2021), along with the production of CO_2 from HCO_3^- in conditions of CO_2 depletion, leads to the generation of OH^- ions (Shiraiwa et al., 1993). This process raises the pH of the system, explaining the marked increase observed under the High treatment condition in Fig. 3B.

Such development agrees with previous observations of PP and cell division decreases paired with increased pH values (up to ~8.8) associated with low DIC availability (Chen and Durbin, 1994; Goldman, 1999), as is the case in this experiment (Fig. 3B). It has been observed that a pH above 8 can reduce the activity of the transmembrane-transporting ATPases responsible for nitrate uptake at the cellular level (Falkowski, 1975). However, there have been hardly any studies where the planktonic community is subjected to CO_2 levels as low as those reached in the Medium and High treatments (Fig. 3C) in the final phase of the present experiment (<1.25 μmol L^{-1}). Hansen (2002) studied the effect of high pH on marine phytoplankton and, comparing with the literature, observed how most of these organisms significantly reduced their production and growth rates above pH 8 due to low availability of DIC as CO_2. Such conditions have also been observed to produce alterations in internal regulation and membrane transport processes at these pH ranges (Smith and Raven, 1979). In addition, Humphrey (1975) identified growth limitations in *Chaetoceros dudymus* at pH values of 9, and this diatom genus was one of the most abundant identified by Bach et al. (2019a) in an experiment with a planktonic community similar to the present study. Thus, the reduction in PP, Chl-a, biomass and nutrient uptake after day 11 in the High treatment may be closely related to the DIC limitation and pH increase observed in this treatment, causing the subsequent abnormal nutrient accumulation (Fig. 5B).

The lower air-water diffusivity in the mesocosm, due to the reduced area in contact with the atmosphere compared to the water column (Riebesell et al., 2013), must be considered when extrapolating these results to realistic conditions of nutrient discharge. Changes in pH as a result of excessive DIC consumption would not be as severe in open waters with a large gas exchange surface area and high hydrodynamics due to the higher diffusion flux of CO_2 (Fick, 1855). However, the experiment illustrates how elevated nutrient inputs at the onset of eutrophication events can increase DIC fixation until depletion, promoting the diffusion of carbon from the atmosphere to the ocean and thus enhancing an atmospheric CO_2 sink (Abril et al., 2022). As observed in the High treatment of this experiment, if the coastal water mass lacks sufficient diffusion to prevent a sharp decrease in CO_2, leading to limitations in primary production and phytoplankton growth, nutrient accumulation from the effluent can occur. In addition to the effects associated with the pH increase in the planktonic community (Chen and Durbin, 1994; Goldman, 1999; Hansen, 2002; Pedersen and Hansen, 2003), an extension of the area affected by the horizontal diffusion of these nutrients would be expected (Valiela et al., 1990), which would aggravate their effects and consequently their management.

4.2. Sustained high production at low inorganic carbon

Despite the fact that the Medium treatment received a lower daily nutrient concentration compared to the High treatment, the community was able to maintain high and stable values of PP, biomass, and Chl-a throughout the entire experiment. However, similar to the High treatment, the Medium treatment also experienced significant consumption of CO_2 by phytoplankton (Fig. 3C), reaching similar values of CO_2 concentration (<1.25 μmol L^{-1}) in the final phase of the experiment. The rate of CO_2 consumption played a crucial role in achieving this stability in the community's production. While the High treatment took only 5 days to decrease CO_2 levels from near 10 μmol L^{-1} to an average lower than 1.25 μmol L^{-1}, the Medium treatment required three times longer, providing the phytoplankton community with a longer period to acclimate to the new DIC availability. Torstensson et al. (2015) highlighted the importance of long-term acclimation for significant physiological changes related to DIC availability in the growth and production of the diatom species *Nitzschia lecointei*, while short-term studies found no differences or even negative effects (Torstensson et al., 2012, 2013).

Torstensson et al. (2015) identified a positive adaptation of these diatoms to such changes. An indication of the phytoplankton community's acclimation in the Medium treatment is the relative stability observed in the biomass of different phytoplankton groups after day 7 (Figs. 9 and 10C). In contrast, in the High treatment, organisms with more mixotrophic behaviors, such as dinoflagellates and larger nano-eukaryotes (Chan et al., 2009; Livanou et al., 2019; Ptacnik et al., 2016), increased their presence with the decline in diatom biomass (Fig. 10D). Another aspect that reveals the stability in the planktonic community of the Medium treatment compared to the High treatment is the evolution of zooplankton biomass during the experiment (Fig. 11). Despite the differential increase in biomass in both fractions of the High treatment, the reduction in biomass across almost all phytoplankton groups, along with the extreme pH reached in the second half of the experiment (above 9), led to a decline in biomass for both groups in this treatment. However, the Medium treatment managed to maintain a positive trend in the microzooplankton fraction, despite also reaching high pH levels (above 8.5) in the second half of the experiment. Pedersen and Hansen (2003) observed during high pH incubations that copepods (mesozooplankton) are more sensitive than ciliates and protozooplankton (microzooplankton) to pH values above 9. This difference in sensitivity may explain why the declines in biomass are more pronounced in the evolution of mesozooplankton biomass (Fig. 11A), compared to microzooplankton, which appears to delay its decrease (Fig. 11B).

One key factor influencing DIC consumption is the balance between the availability of different nutrients. Verschoor et al. (2013) observed that when CO_2 concentration is not increased in mesocosm cultures with nutrient additions, a depletion of CO_2 occurs following the algal bloom, resulting in a sudden rise in pH. Taucher et al. (2017) observed that the differences in DIC uptake rates between two diatom species began to appear at low CO_2 concentrations (below 10 μmol L^{-1}) when nutrient limitation occurred, suggesting that inhibition of DIC assimilation at low CO_2 played an important role in the observed response. Other studies have reported that growth inhibition due to low CO_2 availability occurs below a threshold of 5–7.5 μmol L^{-1}. However, in our experiment, the Medium treatment was able to maintain stability with constant production until the end, reaching a minimum value of 1.03 μmol L^{-1} on day 27. In contrast, the High treatment fell below this concentration starting from day 13 onwards. Therefore, we suggest that the CO_2 threshold for this phytoplankton community, dominated by diatoms, is approximately 1 μmol L^{-1}. Diatoms are efficient photosynthetic organisms with advantageous adaptations, such as using HCO_3^- instead of CO_2 when the latter is limited (Nimer et al., 1997). Some studies demonstrate that certain diatom species, such as *Skeletonema costatum*, are capable of sustaining high photosynthetic activity under low CO_2 conditions (<4.5 μmol kg^{-1}) and high pH levels (>8.5). This ability is attributed to increased activity of the enzyme carbonic anhydrase, which enables the utilisation of HCO_3^- as a source of inorganic carbon when CO_2 is limiting but nitrate and phosphate are non-limiting (Gao et al., 2018a, 2018b). This mechanism may explain how the Medium treatment group was able to maintain primary production rates despite low CO_2 levels observed at the end of the experiment, in contrast to the High treatment group, which could not adapt in this manner and consequently experienced a collapse at higher pH and lower CO_2 levels.

There are no studies focused on the threshold levels of HCO_3^- that diatoms can uptake under highly carbon-limited conditions. However,

in this study, we observe that after reaching a minimum HCO_3^- concentration of 600 μmol L^{-1} in the High treatment (Fig. 3D), the levels began to increase slightly but in a greater manner than CO_2 (Fig. 3C). This could suggest a minimum threshold for bicarbonate utilisation by the diatom community. Aside from the limitation due to DIC, another factor that may have led to the collapse of the diatom community in the experiment is the reduction in the efficiency of frustule silicification caused by high pH and TA values. This phenomenon has been observed in other studies focusing on Ocean Alkalinity Enhancement (OAE), where treatments with increased alkalinity have resulted in a decrease in dissolved silicon availability (Gately et al., 2023) and in the production of biogenic silicon (Ferderer et al., 2022). These studies attribute the causes to an increase in the precipitation of silicate-containing minerals, which could hinder uptake by pelagic diatoms, or to alterations in diatom silicification dependent on inorganic carbon speciation. However, other studies have reported contrasting results, where increased alkalinity using silicate-containing minerals enhances the silicification capacity of diatoms (Bach et al., 2019b; Ferderer et al., 2024). In the case of the experiment conducted in this study, the High treatment did not exhibit silicon limitation (Fig. 2D), and therefore, any changes in the carbonate system cannot be attributed to alterations in silicate availability. Nonetheless, other studies have corroborated that silicon deposition vesicles (SDVs) require an acidic environment to facilitate the aggregation and rapid nucleation of silicon particles (Vrieling et al., 1999; Hervé et al., 2012). This could indeed explain why, under very high pH conditions (~9) in the High treatment, diatoms are unable to efficiently form their frustules despite the high availability of dissolved silicon.

These results could have significant implications for the development of OAE methodologies. A substantial increase in TA and pH in the system might reduce primary productivity, potentially destabilizing the marine trophic network. This reduction in productivity could diminish the system's capacity for carbon sequestration, effectively transforming an originally autotrophic system into a predominantly heterotrophic one, as observed in the High treatment of this experiment. Furthermore, this experiment underscores the critical impact of coastal nutrient inputs on local planktonic communities. However, if such inputs are introduced gradually, the timing could mitigate their effects by allowing planktonic organisms to adapt, thereby avoiding physiological thresholds that could disrupt their functionality. This adaptive process promotes stability in community composition, favouring the dominance of efficient autotrophic organisms like diatoms. These organisms play a key role in sustaining the marine trophic web while limiting the proliferation of dinoflagellates, which are often associated with harmful algal blooms (Hallegraeff, 2003). Moreover, maintaining a balanced autotrophic activity could delay oxygen depletion in the water column, mitigating the negative impacts of hypoxia in coastal zones (Oviatt et al., 1986).

4.3. Bacterial remineralization despite nutrients constraints

The majority of DOC released into the environment is mainly created by primary producers (Kirchman et al., 1991; Søndergaard and Middelboe, 1995). Subsequently, HB remineralise it into DIC and produce organic by-products that tend to increase the recalcitrance of the DOM pool (Ducklow et al., 1986; Williams and Druffel, 1987). Despite nitrogen (Control, Low, and Medium) or carbon (High) limitations registered in the different treatments, which resulted in stabilized or reduced primary production (PP) rates and DOC concentrations, bacterial growth remained active in all treatments, leading to an increase in the quantity of CDOM (Fig. 7C and D), with signs of intense microbial transformation (Catalá et al., 2018). This increase in CDOM production leads to a reduction in light availability for primary production, thereby reducing its efficiency in the water column (Urtizberea et al., 2013). Interestingly, although bacterial remineralization persisted throughout the experiment, in the Medium treatment bacterial activity was insufficient to mitigate the accumulation of DOC, unlike the High treatment where diatom communities collapsed by the depletion of DIC (CO_2 and HCO_3^-). This observation suggests that diatoms, which are known to release large quantities of organic compounds (Mühlenbruch et al., 2018), might have been the main sources of DOC in both treatments. A similar pattern was observed with dissolved oxygen evolution (Fig. 3C), where the diatoms, responsible for the initial increase in concentration due to photosynthesis, later collapsed, leading to a deficit reflected in the decrease in oxygen levels until the end of the experiment. As with DOC, this effect was not observed in the Medium treatment, where the diatom community, the main source of oxygen in the system, was maintained. If the High treatment had continued for more than 30 days, bacterial metabolic rate might have decreased in parallel with DOC, leading to a reduction in oxygen consumption mediated by a decrease in primary production (Blight et al., 1995).

Another important aspect of DOC production was that, in the treatments with lower nutrient concentrations (Control and Low), DOC production was as high as, and at times even exceeded, POC production during specific phases of the experiment (from T6 to T9). Studies have shown that in more oligotrophic communities, where phytoplankton is dominated primarily by picoplankton, a significant portion of net primary production is found in the dissolved fraction (Teira et al., 2001). However, as previously mentioned, this dissolved production is also closely linked to the recycling of organic matter by the microbial community, with natural environments showing the highest rates of oceanic DOC production during deep convective overturn (Hansell and Carlson, 1998). This underscores the importance of POC to DOC transfer in the deep ocean, where photosynthesis is limited by light availability. Considering the observed linear increase in HB abundance and recalcitrant organic matter throughout the experiment, it is possible that the containment of the community within mesocosms further promotes this recycling process, thereby increasing DOC production relative to natural conditions.

Under realistic conditions of coastal runoff, nutrients may be discharged directly to the environment in inorganic form, as in the case of waters contaminated by synthetic fertilisers, or in organic forms, such as urban or agricultural wastewater (Paerl, 1999). In the latter case, the dissolved fraction from the organic matter serves as a resource for the microbial community (Deininger and Frigstad, 2019). Therefore, when managing discharges that may lead to eutrophication, it is crucial to study their origin and nature in order to understand how the community may respond to changes in the target environment (Vilmin et al., 2018). Furthermore, the importance of continuous monitoring tracking the microbial evolution of the system (Shen et al., 2013) is a dynamic and invaluable component of effective eutrophication management, as microbial communities play a pivotal role in nutrient cycling and overall ecosystem health (Astudillo-García et al., 2019). Regular monitoring allows early detection of changes in microbial dynamics, providing crucial insights into the resilience of the system and its vulnerability to eutrophication.

5. Conclusions

Several key findings of this study shed light on the complex dynamics of nutrient enrichment and its impact on marine ecosystems. The experiment demonstrated that extreme fertilization led to inorganic carbon depletion (CO_2 and HCO_3^-), particularly in high input conditions, where an imbalance between availability and replenishment triggered a rapid decline in inorganic carbon levels. This depletion, observed between days 7 and 11 in the High treatment, had cascading effects on the planktonic community, resulting in a significant reduction in primary production (PP), chlorophyll (Chl-a), dissolved oxygen, nutrient uptake, and phyto-zoo biomass. This work highlights the importance of considering the balance between nutrient availability and consumption in managing coastal nutrient inputs. The experiment showed that sustained high production at low inorganic carbon levels, as observed in the Medium treatment, was facilitated by the phytoplankton community's

ability to acclimate over a more extended period. The slower decrease in CO_2 allowed for a more stable system, emphasizing the significance of long-term acclimation for physiological changes related to dissolved inorganic carbon (DIC) availability.

The findings also underscored the role of diatoms, which are efficient photosynthetic organisms under non-limiting conditions, in maintaining the stability of the system. Additionally, the work highlights the impact of elevated pH on zooplankton production, revealing varying sensitivity among different fractions. The experiment emphasized the alleviating effect of managing coastal nutrient inputs gradually, allowing planktonic communities to adapt and avoid reaching undesirable ecological thresholds, thereby favouring the dominance of an autotrophic system. Furthermore, the study explored the role of bacterial remineralization in the context of nutrient constraints. Despite nitrogen or carbon limitations, bacterial respiration remained active in all treatments, contributing to the production of chromophoric dissolved organic matter (CDOM). The importance of studying the origin and nature of discharges that may lead to eutrophication was emphasized, particularly in cases where organic matter inputs serve as a resource for the microbial community.

However, mesocosm constraints, such as limited gas exchange, likely intensified CO_2 depletion and pH and TA changes, making further research in open-water settings necessary to validate these findings under natural hydrodynamic conditions. Extending experiment durations could also clarify long-term impacts on oxygen, pH, and inorganic carbon levels in eutrophic systems. Moving forward, improved understanding of nutrient thresholds, resilience and recovery processes. Additionally, long-term and large-scale experiments examining high alkalinity and low CO_2 conditions would enhance our understanding of the impacts of carbon dioxide removal (CDR) techniques, such as Ocean Alkalinisation Enhancement. These studies could provide deeper insights into the efficiency and ecological effects of such approaches, particularly regarding their influence on marine trophic dynamics and ecosystem stability.

In conclusion, this paper highlights the intricate interactions between different fertilisation conditions, inorganic carbon consumption, planktonic community dynamics, and bacterial remineralization. The findings underscore the importance of nuanced nutrient management strategies, gradual adaptation of planktonic communities, and continuous monitoring to understand and address the complexities of eutrophication in coastal ecosystems.

CRediT authorship contribution statement

Jorge J. Santos-Bruña: Writing – original draft, Visualization, Data curation, Conceptualization. **Nauzet Hernández-Hernández:** Writing – review & editing, Validation, Supervision, Formal analysis, Conceptualization. **María F. Montero:** Software, Methodology, Data curation. **Markel Gómez-Letona:** Writing – review & editing, Software, Methodology, Data curation. **Moritz Baumann:** Writing – review & editing, Resources, Methodology, Data curation. **Jan Taucher:** Writing – review & editing, Resources, Methodology, Data curation. **Carsten Spisla:** Software, Resources, Methodology, Data curation. **Antonia Thielecke:** Software, Resources, Methodology, Data curation. **Andrea Ludwig:** Writing – review & editing, Resources, Methodology, Data curation. **Ulf Riebesell:** Validation, Supervision, Resources, Project administration, Investigation, Funding acquisition, Conceptualization. **Javier Arístegui:** Writing – review & editing, Validation, Supervision, Resources, Formal analysis, Conceptualization.

Funding

This study is a contribution to the Ocean Artificial Upwelling Project (Ocean artUp) funded by an advanced Grant of the European Research Council (N0. 695094) to UR. JA was supported by a Helmholtz International Fellow Award, 2015 (Helmholtz Association, Germany) and by the US National Science Foundation grant OCE-1840868 to the Scientific Committee on Oceanic Research (SCOR, United States) WG 155.

Declaration of competing interest

The authors declare the following financial interests/personal relationships which may be considered as potential competing interests: Javier Aristegui reports article publishing charges and equipment, drugs, or supplies were provided by University of Las Palmas de Gran Canaria. Javier Aristegui reports a relationship with University of Las Palmas de Gran Canaria that includes: employment. If there are other authors, they declare that they have no known competing financial interests or personal relationships that could have appeared to influence the work reported in this paper.

Acknowledgments

The authors thank the Plataforma Oceánica de Canarias (PLOCAN) for their extensive support throughout the experiment, including the use of their facilities and their assistance during the sampling of the mesocosms. We especially thank the whole KOSMOS team (GEOMAR) for logistic and technical work, as well as the Group of Biological Oceanography (GOB-IOCAG, ULPGC) for providing lab facilities and technical support.

Data availability

The authors do not have permission to share data.

References

Abril, G., Cotovicz Jr, L.C., Nepomuceno, A., Erbas, T., Costa, S., Ramos, V.V., Knoppers, B.A., 2022. Spreading eutrophication and changing CO2 fluxes in the tropical coastal ocean: A few lessons from rio de janeiro. Acmar 55 (Especial), 461–476.

Alcántara, C., Posadas, E., Guieysse, B., Muñoz, R., 2015. Microalgae-based wastewater treatment. Handbook of Marine Microalgae. Elsevier, pp. 439–455.

Anabalón, V., Arístegui, J., Morales, C.E., Andrade, I., Benavides, M., Correa-Ramírez, M. A., Orbi, A., 2014. The structure of planktonic communities under variable coastal upwelling conditions off cape ghir (31°N) in the canary current system (NW africa). Prog. Oceanogr. 120, 320. https://doi.org/10.1016/j.pocean.2013.10.015.

Astudillo-García, C., Hermans, S.M., Stevenson, B., Buckley, H.L., Lear, G., 2019. Microbial assemblages and bioindicators as proxies for ecosystem health status: potential and limitations. Appl. Microbiol. Biotechnol. 103, 6407–6421.

Bach, L.T., Hernández-Hernández, N., Taucher, J., Spisla, C., Sforna, C., Riebesell, U., Arístegui, J., 2019a. Effects of elevated CO 2 on a natural diatom community in the subtropical NE atlantic. Front. Mar. Sci. 6, 75.

Bach, L.T., Gill, S.J., Rickaby, R.E., Gore, S., Renforth, P., 2019b. CO2 removal with enhanced weathering and ocean alkalinity enhancement: potential risks and co-benefits for marine pelagic ecosystems. Frontiers in Climate 1, 476698.

Baños, I., Arístegui, J., Benavides, M., Gómez-Letona, M., Montero, M.F., Ortiz, J., Riebesell, U., 2022. Response of plankton community respiration under variable simulated upwelling events. Front. Mar. Sci. 9, 1006010. https://doi.org/10.3389/fmars.2022.1006010.

Baumann, M., Taucher, J., Paul, A.J., Heinemann, M., Vanharanta, M., Bach, L.T., Hernández-Hernández, N., 2021. Effect of intensity and mode of artificial upwelling on particle flux and carbon export. Front. Mar. Sci. 8, 742142.

Benkeblia, N., Radeva, D., 2018. Climate change and resilience of agroecosystems : mitigation through agroforestry, permaculture, and perennial polyculture systems. Climate Change and Crop Production 105–130. https://doi.org/10.1201/9781315391861-7.

Bjørnsen, P.K., 1986. Automatic determination of bacterioplankton biomass by image analysis. Appl. Environ. Microbiol. 51 (6), 1199–1204.

Blight, S.P., Bentley, T.L., Lefevre, D., Robinson, C., Rodrigues, R., Rowlands, J., Williams, P.l., 1995. Phasing of autotrophic and heterotrophic plankton metabolism in a temperate coastal ecosystem. Mar. Ecol. Prog. Ser. 128, 61–75.

Boxhammer, T., Bach, L.T., Czerny, J., Riebesell, U., 2016. Sampling and processing of mesocosm sediment trap material for quantitative biogeochemical analysis. Biogeosciences 13 (9), 2849–2858.

Børsheim, K.Y., Bratbak, G., 1987. Cell volume to cell carbon conversion factors for a bacterivorous monas sp. enriched from seawater. Mar. Ecol. Prog. Ser. 171–175.

Catalá, T.S., Martínez-Pérez, A.M., Nieto-Cid, M., Álvarez, M., Otero, J., Emelianov, M., Álvarez-Salgado, X.A., 2018. Dissolved organic matter (DOM) in the open mediterranean sea. I. basin–wide distribution and drivers of chromophoric DOM. Prog. Oceanogr. 165, 35–51.

Chan, Y., Tsai, A., Chiang, K., Hsieh, C., 2009. Pigmented nanoflagellates grazing on synechococcus: seasonal variations and effect of flagellate size in the coastal ecosystem of subtropical western pacific. Microb. Ecol. 58, 548–557.
Chen, C.Y., Durbin, E.G., 1994. Effects of pH on the growth and carbon uptake of marine phytoplankton. Mar. Ecol. Prog. Ser. 109, 83.
Correll, D.L., 1998. The role of phosphorus in the eutrophication of receiving waters: a review. J. Environ. Qual. 27 (2), 261. https://doi.org/10.2134/jeq1998.00472425002700020004x.
Deininger, A., Frigstad, H., 2019. Reevaluating the role of organic matter sources for coastal eutrophication, oligotrophication, and ecosystem health. Front. Mar. Sci. 6, 210.
Delgado, J.D., Riera, R., 2020. Anthropogenic disturbances and conservation of coastal environments in an oceanic archipelago. Journal of Integrated Coastal Zone Management 20 (4), 249–264. https://doi.org/10.5894/RGCI-N267.
Dickson, A.G., Millero, F.J., 1987. A comparison of the equilibrium constants for the dissociation of carbonic acid in seawater media. Deep Sea Research Part A. Oceanographic Research Papers 34 (10), 1733–1743.
Duarte, C.M., Agusti, S., Agawin, N.S., 2000. Response of a mediterranean phytoplankton community to increased nutrient inputs: a mesocosm experiment. Mar. Ecol. Prog. Ser. 195, 61–70.
Ducklow, H.W., Purdie, D.A., Williams, P.J.L., Davies, J.M., 1986. Bacterioplankton: a sink for carbon in a coastal marine plankton community. Science 232 (4752), 865–867.
EU monitor. Directive 1991/676. Retrieved from: https://www.eumonitor.eu/9353000/1/j4nvk6yhcbpeywk_j9vvik7m1c3gyxp/vitgbghm8hxi.
Falkowski, P.G., 1975. Nitrate uptake in marine phytoplankton: comparison of half-saturation constants from seven species 1. Limnol. Oceanogr. 20 (3), 412–417.
Ferderer, A., Chase, Z., Kennedy, F., Schulz, K.G., Bach, L.T., 2022. Assessing the influence of ocean alkalinity enhancement on a coastal phytoplankton community. Biogeosciences 19 (23), 5375–5399.
Ferderer, A., Schulz, K.G., Riebesell, U., Baker, K.G., Chase, Z., Bach, L.T., 2024. Investigating the effect of silicate-and calcium-based ocean alkalinity enhancement on diatom silicification. Biogeosciences 21 (11), 2777–2794.
Feng, Y., Xiong, Y., Hall-Spencer, J.M., Liu, K., Beardall, J., Gao, K., et al., 2024. Shift in algal blooms from micro-to macroalgae around China with increasing eutrophication and climate change. Global Change Biol. 30 (1), e17018.
Ferriol, C., Miracle, M.R., Vicente, E., 2016. Effects of nutrient addition, recovery thereafter and the role of macrophytes in nutrient dynamics of a mediterranean shallow lake: a mesocosm experiment. Mar. Freshw. Res. 68 (3), 506–518.
Fick, A., 1855. V. on liquid diffusion. London, Edinburgh Dublin Phil. Mag. J. Sci. 10 (63), 30–39.
Gao, G., Xia, J., Yu, J., Zeng, X., 2018a. Physiological response of a red tide alga (Skeletonema costatum) to nitrate enrichment, with special reference to inorganic carbon acquisition. Mar. Environ. Res. 133, 15–23.
Gao, G., Xia, J., Yu, J., Fan, J., Zeng, X., 2018b. Regulation of inorganic carbon acquisition in a red tide alga (Skeletonema costatum): the importance of phosphorus availability. Biogeosciences 15 (16), 4871–4882.
Gately, J.A., Kim, S.M., Jin, B., Brzezinski, M.A., Iglesias-Rodriguez, M.D., 2023. Coccolithophores and diatoms resilient to ocean alkalinity enhancement: a glimpse of hope? Sci. Adv. 9 (24), eadg6066.
Glibert, P., Burford, M., 2017. Globally changing nutrient loads and harmful algal blooms: recent advances, new paradigms, and continuing challenges. Oceanography 30 (1), 58. https://doi.org/10.5670/oceanog.2017.110.
Goldman, J.C., 1999. Inorganic carbon availability and the growth of large marine diatoms. Mar. Ecol. Prog. Ser. 180, 81–91.
Gómez-Letona, M., Sebastián, M., Baños, I., Montero, M.F., Barrancos, C.P., Baumann, M., Arístegui, J., 2022. The importance of the dissolved organic matter pool for the carbon sequestration potential of artificial upwelling. Front. Mar. Sci. 9, 969714. https://doi.org/10.3389/fmars.2022.969714.
Grasshoff, K., Kremling, K., Ehrhardt, M., 2009. Methods of Seawater Analysis. John Wiley & Sons.
Hallegraeff, G.M., 2003. Harmful algal blooms: a global overview. Manual on Harmful Marine Microalgae 33, 1–22.
Hansell, D.A., Carlson, C.A., 1998. Net community production of dissolved organic carbon. Global Biogeochem. Cycles 12 (3), 443–453.
Hansen, H.P., Grasshoff, K., 1983. In: Grasshoff, K., Ehrhardt, M., Kremling, K. (Eds.), Procedures for the Automated Determination of Seawater Constituents, second ed., Methods of Seawater Analysis. Verlag Chemie, Weinheim, pp. 362–379.
Hansen, P.J., 2002. Effect of high pH on the growth and survival of marine phytoplankton: implications for species succession. Aquat. Microb. Ecol. 28 (3), 279–288.
Helms, J.R., Stubbins, A., Ritchie, J.D., Minor, E.C., Kieber, D.J., Mopper, K., 2008. Absorption spectral slopes and slope ratios as indicators of molecular weight, source, and photobleaching of chromophoric dissolved organic matter. Limnol. Oceanogr. 53 (3), 955–969.
Hernández-Hernández, N., Bach, L.T., Montero, M.F., Taucher, J., Baños, I., Guan, W., Arístegui, J., 2018. High CO2 under nutrient fertilization increases primary production and biomass in subtropical phytoplankton communities: a mesocosm approach. Front. Mar. Sci. 5 (JUN), 380556. https://doi.org/10.3389/fmars.2018.00213.
Hervé, V., Derr, J., Douady, S., Quinet, M., Moisan, L., Lopez, P.J., 2012. Multiparametric analyses reveal the pH-dependence of silicon biomineralization in diatoms. PLoS One 7 (10), e46722.
Holmes, R.M., Aminot, A., Kérouel, R., Hooker, B.A., Peterson, B.J., 1999. A simple and precise method for measuring ammonium in marine and freshwater ecosystems. Can. J. Fish. Aquat. Sci. 56 (10), 1801–1808.
Holm-Hansen, O., Lorenzen, C.J., Holmes, R.W., Strickland, J.D., 1965. Fluorometric determination of chlorophyll. ICES. Journal of Marine Science 30 (1), 3–15.
Howarth, R.W., 2008. Coastal nitrogen pollution: a review of sources and trends globally and regionally. Harmful Algae 8 (1), 14. https://doi.org/10.1016/j.hal.2008.08.015.
Howarth, R.W., Marino, R., 2006. Nitrogen as the limiting nutrient for eutrophication in coastal marine ecosystems: evolving views over three decades. Limnol. Oceanogr. 51 (1 II), 364–376. https://doi.org/10.4319/LO.2006.51.1_PART_2.0364.
Humphrey, G.F., 1975. The photosynthesis: respiration ratio of some unicellular marine algae. J. Exp. Mar. Biol. Ecol. 18 (2), 111–119.
ISTAC. Gobierno de canarias. Retrieved from https://www3.gobiernodecanarias.org/istac/statistical-visualizer/visualizer/data.html?resourceId=be85e239-12f1-46c9-b42f-3533d27d03ce&indicatorSystem=C00075B&resourceType=indicatorInstance#visualization/table.
Jerez-Darias, L.M., García-Cruz, J.I., 2024. Los desequilibrios geodemográficos en canarias: Una expresión de su especialización económica. Boletín De La Asociación De Geógrafos Españoles (98). https://doi.org/10.21138/bage.3443.
Joint, I., Henriksen, P., Fonnes, G.A., Bourne, D., Thingstad, T.F., Riemann, B., 2002. Competition for inorganic nutrients between phytoplankton and bacterioplankton in nutrient manipulated mesocosms. Aquat. Microb. Ecol. 29 (2), 145–159.
Kirchman, D.L., Suzuki, Y., Garside, C., Ducklow, H.W., 1991. High turnover rates of dissolved organic carbon during a spring phytoplankton bloom. Nature 352 (6336), 612–614.
Lagus, A., Suomela, J., Helminen, H., Lehtimäki, J.M., Sipura, J., Sivonen, K., Suominen, L., 2007. Interaction effects of N: P ratios and frequency of nutrient supply on the plankton community in the northern baltic sea. Mar. Ecol. Prog. Ser. 332, 77–92.
Lin, T., Gibson, V., Cui, S., Yu, C., Chen, S., Ye, Z., Zhu, Y., 2014. Managing urban nutrient biogeochemistry for sustainable urbanization. Environ. Pollut. 192, 244. https://doi.org/10.1016/j.envpol.2014.03.038.
Livanou, E., Lagaria, A., Santi, I., Mandalakis, M., Pavlidou, A., Lika, K., Psarra, S., 2019. Pigmented and heterotrophic nanoflagellates: abundance and grazing on prokaryotic picoplankton in the ultra-oligotrophic eastern mediterranean sea. Deep Sea Res. Part II Top. Stud. Oceanogr. 164, 100–111.
Mehrbach, C., Culberson, C.H., Hawley, J.E., Pytkowicx, R.M., 1973. Measurement of the apparent dissociation constants of carbonic acid in seawater at atmospheric pressure 1. Limnol. Oceanogr. 18 (6), 897–907.
Menden-Deuer, S., Lessard, E.J., 2000. Carbon to volume relationships for dinoflagellates, diatoms, and other protist plankton. Limnol. Oceanogr. 45 (3), 569–579.
Mieczan, T., Adamczuk, M., Pawlik-Skowrońska, B., Toporowska, M., 2015. Eutrophication of peatbogs: consequences of P and N enrichment for microbial and metazoan communities in mesocosm experiments. Aquat. Microb. Ecol. 74 (2), 121–141.
Mühlenbruch, M., Grossart, H., Eigemann, F., Voss, M., 2018. Mini-review: phytoplankton-derived polysaccharides in the marine environment and their interactions with heterotrophic bacteria. Environ. Microbiol. 20 (8), 2671–2685.
Murphy, J., Riley, J.P., 1962. A modified single solution method for the determination of phosphate in natural waters. Anal. Chim. Acta 27, 31–36.
Nimer, N.A., Iglesias-Rodriguez, M.D., Merrett, M.J., 1997. Bicarbonate utilization by marine phytoplankton species. J. Phycol. 33 (4), 625–631.
Olenina, I., 2006. Biovolumes and Size-Classes of Phytoplankton in the Baltic Sea.
Ortiz, J., Arístegui, J., Hernández-Hernández, N., Fernández-Méndez, M., Riebesell, U., 2022. Oligotrophic phytoplankton community effectively adjusts to artificial upwelling regardless of intensity, but differently among upwelling modes. Front. Mar. Sci. 9, 880550.
Oviatt, C.A., Keller, A.A., Sampou, P.A., Beatty, L.L., 1986. Patterns of productivity during eutrophication: a mesocosm experiment. Mar. Ecol. Prog. Ser. 28 (1–2), 69–80.
Paerl, H.W., 1999. Cultural eutrophication of shallow coastal waters: coupling changing anthropogenic nutrient inputs to regional management approaches. Limnologica 29 (3), 249–254.
Pedersen, M.F., Hansen, P.J., 2003. Effects of high pH on the growth and survival of six marine heterotrophic protists. Mar. Ecol. Prog. Ser. 260, 33–41.
Pierrot, D., Lewis, E., Wallace, D.W.R., 2006. CO2SYS DOS Program developed for CO2 system calculations. ORNL/CDIAC-105. Carbon Dioxide Information Analysis Center. Oak Ridge National Laboratory, US Department of Energy, Oak Ridge, TN.
Ptacnik, R., Gomes, A., Royer, S., Berger, S.A., Calbet, A., Nejstgaard, J.C., Ptacnikova, R., 2016. A light-induced shortcut in the planktonic microbial loop. Sci. Rep. 6 (1), 29286.
Rabalais, N.N., Turner, R.E., Díaz, R.J., Justić, D., 2009. Global change and eutrophication of coastal waters. ICES (Int. Counc. Explor. Sea) J. Mar. Sci. 66 (7), 1528–1537.
Riebesell, U., Czerny, J., von Bröckel, K., Boxhammer, T., Büdenbender, J., Deckelnick, M., Lentz, U., 2013. A mobile sea-going mesocosm system–new opportunities for ocean change research. Biogeosciences 10 (3), 1835–1847.
Santamarta, J.C., Miklin, L., Gomes-Nadal, C.O., Rodríguez-Alcántara, J.S., Rodríguez-Martín, J., Cruz-Pérez, N., 2023. Waste management and territorial impact in the canary islands. Land 12 (1). https://doi.org/10.3390/land12010212.
Schützenmeister, A., Jensen, U., Piepho, H., 2012. Checking normality and homoscedasticity in the general linear model using diagnostic plots. Commun. Stat. Simulat. Comput. 41 (2), 141–154.
Sharp, J.H., 1974. Improved analysis for "particulate" organic carbon and nitrogen from seawater 1. Limnol. Oceanogr. 19 (6), 984–989.
Sharp, J.H., Benner, R., Bennett, L., Carlson, C.A., Dow, R., Fitzwater, S.E., 1993. Re-evaluation of high temperature combustion and chemical oxidation measurements of dissolved organic carbon in seawater. Limnol. Oceanogr. 38 (8), 1774–1782.

Shen, Z., Niu, J., Wang, Y., Wang, H., Zhao, X., Shen, Z., Zhao, X., 2013. Eutrophication Risk Assessment. Distribution and Transformation of Nutrients and Eutrophication in Large-Scale Lakes and Reservoirs: the Three Gorges Reservoir, pp. 161–177.

Shiraiwa, Y., Goyal, A., Tolbert, N.E., 1993. Alkalization of the medium by unicellular green algae during uptake dissolved inorganic carbon. Plant Cell Physiol. 34 (5), 649–657.

Smith, F.A., Raven, J.A., 1979. Intracellular pH and its Regulation.

Søndergaard, M., Middelboe, M., 1995. A cross-system analysis of labile dissolved organic carbon. Marine Ecology Progress Series.Oldendorf 118 (1), 283–294.

Taucher, J., Bach, L.T., Boxhammer, T., Nauendorf, A., The Gran Canaria KOSMOS Consortium, Achterberg, E.P., Algueró-Muñiz, M., Arístegui, J., Czerny, J., Esposito, M., Guan, W., Haunost, M., Horn, H.G., Ludwig, A., Meyer, J., Spisla, C., Sswat, M., Stange, P., Riebesell, U., 2017. Influence of ocean acidification and deep water upwelling on oligotrophic plankton communities in the Subtropical North Atlantic: Insights from an *In situ* Mesocosm Study. Front. Mar. Sci 4, 85. https://doi.org/10.3389/fmars.2017.00085.

Teira, E., José Pazó, M., Serret, P., Fernández, E., 2001. Dissolved organic carbon production by microbial populations in the Atlantic Ocean. Limnol. Oceanogr. 46 (6), 1370–1377.

Thomas, C., Cauwet, G., Minster, J., 1995. Dissolved organic carbon in the equatorial atlantic ocean. Mar. Chem. 49 (2–3), 155–169.

Torstensson, A., Chierici, M., Wulff, A., 2012. The influence of increased temperature and carbon dioxide levels on the benthic/sea ice diatom navicula directa. Polar Biol. 35 (2), 205–214.

Torstensson, A., Hedblom, M., Andersson, J., Andersson, M.X., Wulff, A., 2013. Synergism between elevated pCO 2 and temperature on the antarctic sea ice diatom nitzschia lecointei. Biogeosciences 10 (10), 6391–6401.

Torstensson, A., Hedblom, M., Mattsdotter Björk, M., Chierici, M., Wulff, A., 2015. Long-term acclimation to elevated p CO2 alters carbon metabolism and reduces growth in the antarctic diatom nitzschia lecointei. Proc. Biol. Sci. 282 (1815), 20151513.

Urtizberea, A., Dupont, N., Rosland, R., Aksnes, D.L., 2013. Sensitivity of euphotic zone properties to CDOM variations in marine ecosystem models. Ecol. Model. 256, 16–22.

Utermöhl, V.H., 1931. Neue Wege in der quantitativen Erfassung des Plankton.(Mit besonderer Berücksichtigung des Ultraplanktons.) Mit 4 Abbildungen im Text. Internationale Vereinigung für theoretische und angewandte Limnologie: Verhandlungen 5 (2), 567–596.

Valiela, I., Costa, J., Foreman, K., Teal, J.M., Howes, B., Aubrey, D., 1990. Transport of groundwater-borne nutrients from watersheds and their effects on coastal waters. Biogeochemistry 10, 177–197.

Verschoor, A.M., Van Dijk, M.A., Huisman, J., Van Donk, E., 2013. Elevated CO2 concentrations affect the elemental stoichiometry and species composition of an experimental phytoplankton community. Freshw. Biol. 58 (3), 597–611.

Vilmin, L., Mogollón, J.M., Beusen, A.H., Bouwman, A.F., 2018. Forms and subannual variability of nitrogen and phosphorus loading to global river networks over the 20th century. Global Planet. Change 163, 67–85.

Vrieling, E.G., Gieskes, W.W.C., Beelen, T.P., 1999. Silicon deposition in diatoms: control by the pH inside the silicon deposition vesicle. J. Phycol. 35 (3), 548–559.

Williams, P.M., Druffel, E.R., 1987. Radiocarbon in dissolved organic matter in the central north pacific ocean. Nature 330 (6145), 246–248.

Zerveas, S., Mente, M.S., Tsakiri, D., Kotzabasis, K., 2021. Microalgal photosynthesis induces alkalization of aquatic environment as a result of H+ uptake independently from CO2 concentration–New perspectives for environmental applications. J. Environ. Manag. 289, 112546.

Zimmerman, D.W., Zumbo, B.D., 1993. Relative power of the wilcoxon test, the friedman test, and repeated-measures ANOVA on ranks. J. Exp. Educ. 62 (1), 75–86.